

1 Tracking the uptake of labelled host-derived extracellular vesicles by the human fungal pathogen *Aspergillus* 2 *fumigatus*.

4 Corissa Visser^{1,2}, Flora Rivieccio^{1,2}, Thomas Krüger¹, Franziska Schmidt^{1,2}, Zoltán Cseresnyés³, Manfred Rohde⁴,
5 Marc Thilo Figge^{2,3,6}, Olaf Kniemeyer¹, Matthew G. Blango^{5*}, Axel A. Brakhage^{1,2,6*}

⁷ ¹ Department of Molecular and Applied Microbiology, Leibniz Institute for Natural Product Research and
⁸ Infection Biology—Hans Knöll Institute (Leibniz-HKI), Jena, Germany.

⁹ ²Institute of Microbiology, Friedrich Schiller University, Jena, Germany.

10 ³ Research Group Applied Systems Biology, Leibniz Institute for Natural Product Research and Infection Biology
11 (HKI), Jena, Germany

12 · Helmholtz Centre for Infection Research (HZI), Braunschweig, Germany.

⁵ Junior Research Group RNA Biology of Fungal Infections, Leibniz Institute for Natural Product Research and Infection Biology (Leibniz-HKI), Jena, Germany.

¹⁵ ⁶Excellence Cluster *Balance of the Microverse*, Friedrich Schiller University, Jena, Germany.

17 **Running Title:** Genetic-based reporter system for labelling host EVs

18 **Key Words:** Extracellular vesicles, A549 epithelial cells, Nanoluciferase, green fluorescent protein, CD63, CD81,
19 CD9, *Aspergillus fumigatus*

*Corresponding authors: Correspondence: E-mail: axel.brakhage@leibniz-hki.de

22 Tel. +49 (0)3641-532 1001

25 **ABSTRACT**

26 Extracellular vesicles (EVs) have gained attention as facilitators of intercellular as well as interkingdom
27 communication during host-microbe interactions. Recently we showed that upon infection, host
28 polymorphonuclear leukocytes produce antifungal EVs targeting the clinically important fungal pathogen
29 *Aspergillus fumigatus*; however, the small size of EVs (< 1 µm) complicates their functional analysis. Here, we
30 employed a more tractable, reporter-based system to label host alveolar epithelial cell-derived EVs and enabled
31 their visualisation during *in vitro* *A. fumigatus* interaction. Fusion of EV marker proteins (CD63, CD9, and CD81)
32 with a Nanoluciferase (NLuc) and a green fluorescent protein (GFP) facilitated their relative quantification by
33 luminescence and visualization by a fluorescence signal. The use of an NLuc fused with a GFP is advantageous as
34 it allows for quantification and visualisation of EVs simultaneously without additional external manipulation and
35 to distinguish subpopulations of EVs. Using this system, visualisation and tracking of EVs was possible using
36 confocal laser scanning microscopy and advanced imaging analysis. These experiments revealed the propensity
37 of host cell-derived EVs to associate with the fungal cell wall and ultimately colocalize with the cell membrane of
38 *A. fumigatus* hyphae in large numbers. In conclusion, we have created a series of tools to better define the
39 complex interplay of host-derived EVs with microbial pathogens.

40 **INTRODUCTION**

41 Human pathogenic fungi continue to pose a global threat, especially to immunocompromised individuals and
42 those with underlying diseases such as leukemia, chronic obstructive pulmonary disease, or severe influenza,
43 (Köhler *et al.* 2017; WHO 2022; Denning 2024). In the recent World Health Organization fungal priority pathogen
44 list, the ubiquitously distributed, filamentous saprobe *Aspergillus fumigatus* was added to the critical priority
45 group due to its ability to cause disease ranging from allergic reactions to life-threatening invasive aspergillosis
46 in immunocompromised hosts (Brakhage 2005; van de Veerdonk *et al.* 2017; Latgé *et al.* 2019; WHO 2022).
47 *A. fumigatus* typically undergoes propagation through the asexual production of spores called conidia (Latgé *et*
48 *al.* 2019). With their small size of only 2-3 µm in diameter and their hydrophobic surface structure, conidia are
49 dispersed through the air and can be easily inhaled. In the lungs, they can reach the alveoli, where they are
50 rapidly cleared by innate immune cells in immunocompetent hosts, but able to germinate, form hyphae, and
51 cause invasive fungal growth in immunocompromised patients (Heinekamp *et al.* 2015).

52 During infection, both professional phagocytic immune cells (Lionakis *et al.* 2023) and lung epithelial
53 cells (Amin *et al.* 2014; Ewald *et al.* 2021; Jia *et al.* 2023) are required for the coordinated clearance of
54 *A. fumigatus* conidia from the lungs. In recent years, extracellular vesicles (EVs) have gained attention for
55 facilitating communication between human cells or between hosts and microorganisms; however, the potential
56 role of host-derived EVs during *A. fumigatus* infection remains largely unexplored. Recently it was shown that
57 upon infection, host polymorphonuclear leukocytes (PMNs) produce EVs distinct from those released during a
58 healthy state and that are able to inhibit *A. fumigatus* conidia and hyphae (Shopova *et al.* 2020). EVs are a
59 heterogenous group of membrane-delimited vesicles secreted by almost all cell types that play important roles
60 in cell-to-cell communication during physiological and pathological states (Brakhage *et al.* 2021). Classification of
61 EVs into subtypes is difficult and currently distinction is mostly based on their type of biogenesis, resulting in
62 three primary subgroups named exosomes, ectosomes/microvesicles, and apoptotic bodies (Abels *et al.* 2016;
63 van Niel *et al.* 2018; Brakhage *et al.* 2021). Apoptotic bodies are a heterogenous group of vesicles associated
64 with cell death and are frequently considered a confounding factor in studies of EVs in otherwise healthy cells
65 (Kakarla *et al.* 2020), and even more challenging to assess during infection situations. Exosomes are produced in
66 the endosomal pathway by invagination and subsequent inward budding and fission of the limiting membrane
67 of endosomes to form intraluminal vesicles (ILVs). During the maturation process from early to late endosomes,
68 these structures accumulate several ILVs, leading to the generation of multivesicular bodies (MVBs). MVBs are
69 then either directed to lysosomes for degradation of their contents or fused with the cell cytoplasmic membrane
70 releasing the ILVs as exosomes into the extracellular space. Ectosomes are formed through direct outward
71 budding and fission of the cytoplasmic membrane (Abels *et al.* 2016; van Niel *et al.* 2018; Brakhage *et al.* 2021).

EVs carry a wide variety of cargo molecules that can elicit specific cellular functions in the recipient cell, including proteins, lipids, polysaccharides, and nucleic acids (Yáñez-Mó *et al.* 2015). In comparison to spontaneously produced EVs, EVs produced by *A. fumigatus*-infected PMNs were shown to be larger in size and exhibit a higher enrichment of the tetraspanin CD63 in their membranes, as well as a more diverse protein cargo and specifically, larger amounts of proteins and peptides displaying antimicrobial activity. Challenging *A. fumigatus* hyphae with such infection-derived EVs resulted in the localization of the EVs to or within the cell wall as well as infrequently to the cytoplasm of the hyphae, which ultimately resulted in the damage and apparent death of the fungus (Shopova *et al.* 2020).

There are numerous studies on labeling EVs in the literature, either using lipophilic dyes such as DiR (Lázaro-Ibáñez *et al.* 2021), radionucleotide labelling (Lázaro-Ibáñez *et al.* 2021), or tagging of proteins commonly associated with EVs (Hikita *et al.* 2018; Cashikar *et al.* 2019; Gupta *et al.* 2020; Hikita *et al.* 2020; Levy *et al.* 2020; Lázaro-Ibáñez *et al.* 2021). Many of these methods either enabled the detection and quantification of EVs *in vitro* as well as *in vivo*, or their visualization, whereas others combined different fusion proteins to allow both detection and visualization simultaneously (Shpigelman *et al.* 2021). In this study we sought to build on these works by creating a system that would allow for easy detection and visualization of EVs independent of external labelling and thus potential alteration of their behavior. Therefore, we labelled host cell-derived EVs by genetically fusing the commonly accepted EV marker proteins CD63, CD9, and CD81 with a Nanoluciferase (NLuc) luminescence reporter as well as an appropriate fluorescent protein tag. The resulting constructs were transiently transfected into the human lung epithelial cell line A549. EVs isolated from these cells can be detected and visualized through measurement of the luminescence signal in cell culture supernatants and by confocal laser scanning microscopy (CLSM), respectively. We used this system to track host-derived EVs upon coincubation with *A. fumigatus* and revealed robust association of these labeled EVs with fungal hyphae, establishing a system for future dissections of the role of EVs in cross-kingdom delivery of molecules from host to pathogen.

RESULTS

***A. fumigatus*-infected A549 cells secrete EVs associated with well-characterized tetraspanins.**

We selected an *in vitro* cellular system fulfilling two requirements, *i.e.*, it was relevant to fungal infection and readily transfectable, to establish a toolkit for the further study of host-derived EVs. A549 lung epithelial cells met both demands, as they have a history as a cell culture infection model for *A. fumigatus* and are routinely transfected with high efficiency (Jia *et al.* 2023). First, we examined the secretion of EVs by A549 epithelial cells under normal culture conditions and after infection with opsonized *A. fumigatus* conidia, a condition known to

104 elicit antifungal EVs in other systems (Shopova *et al.* 2020; Rafiq *et al.* 2022). Spontaneously released EVs (EVs)
105 from uninfected cells and *A. fumigatus* infection-derived EVs (idEVs) produced by cells challenged with conidia
106 were isolated from conditioned cell culture media using a combination of low-speed centrifugation,
107 ultrafiltration, and size-exclusion chromatography. While unconditioned media prepared with EV-free FCS did
108 not contain any measurable EV-sized particles (**Sup. Fig. 1a**), isolation of EVs using size-exclusion
109 chromatography resulted in most of the particles being released in fractions 7-9 (**Sup. Fig. 1b**), which were also
110 positive for common EV markers (**Sup. Fig. 1c**). Transmission electron microscopy confirmed the presence of
111 round, cup-shaped structures ranging in size from 50 to 100 nm in sample preparations from both infected and
112 non-infected A549 cells (**Fig. 1a**). Next, the concentration and size of EVs and idEVs isolated at different time
113 points were determined using nanoparticle tracking analysis. We observed a significant increase in the particle
114 concentration in the samples after eight hours of incubation for EVs and idEVs but no differences in the
115 concentration between the two culture conditions (**Fig. 1b**). Similarly, size distributions did not greatly differ
116 between EVs and idEVs after shorter periods of incubation and ranged between about 70-300 nm, with a peak at
117 approximately 110 nm. After eight hours, nanoparticle tracking analysis measurements of idEVs revealed a
118 broader size range of isolated particles in the idEV samples with major peaks at around 120 nm and 140 nm, and
119 a smaller peak at 215 nm that was not observed in the EV group, however still resides within the expected size
120 range for EVs (van Niel *et al.* 2018) (**Fig. 1c**). Cell viability was confirmed to be unaffected by infection using LDH
121 release assays (**Sup. Fig. 1d**).

122 EVs have gained attention with respect to their roles during infections; however, visualization of EVs is
123 limited due to their small sizes. We previously suggested the association and apparent internalization of human
124 primary neutrophil-derived EVs into *A. fumigatus* hyphae using a lipophilic dye (Shopova *et al.* 2020). Here, we
125 aimed to improve on our previous efforts by tagging several previously characterized EV marker proteins with a
126 combination of luciferase and fluorescent protein tags. To aid in selection of suitable EV marker proteins, EVs
127 were isolated from conditioned A549 cell culture medium after a 24-hour incubation period from both infected
128 and uninfected cells by size-exclusion chromatography. The isolated EVs were subjected to LC-MS/MS-based
129 proteomic analysis, revealing 884 unique proteins with 30 and 55 proteins solely found in the EV and idEV
130 sample, respectively (**Dataset S1**). Principal component analysis revealed that these samples were not grossly
131 different, but EV sample 2 was a slight outlier driven by principle component 2 at 5.54% (**Fig. 1d, Sup. Fig. 2a**).
132 We did observe significant differences for a limited number of proteins (**Sup. Fig. 2b**), but in general the
133 proteome of EVs appeared quite similar between the EVs and idEVs, with the most obvious changes occurring as
134 serum proteins (e.g., IGHM, APOA1 increased in the idEVs) likely introduced by the opsonization process of *A.*
135 *fumigatus* conidia prior to infection of the host cells. EVs and idEVs were both tested for their antifungal

136 capacity using an *A. fumigatus* mitochondrial GFP reporter strain (Ruf *et al.* 2018) in a host cell-free system as
137 previously described for PMNs (Shopova *et al.* 2020) and PLB-985 cells (Rafiq *et al.* 2022), in which *A. fumigatus*
138 germlings are challenged with isolated EVs for 16 hours, followed by the evaluation of the mitochondrial
139 network integrity. In our assay, in both cases the mitochondrial network appeared largely intact and similar to
140 the untreated growth control, suggesting that EVs isolated from naïve or *A. fumigatus*-infected A549 cells are
141 not overtly antifungal against *A. fumigatus* (**Sup. Fig. 3**). This finding might not be surprising as A549 EVs lacked
142 most of the antimicrobial proteins previously detected in PMN EVs (Shopova *et al.* 2020). We were able to
143 confirm the presence of the three tetraspanins CD9, CD81, and CD63 that are generally accepted EV marker
144 proteins. Although the nuclear lamina protein, lamin A (LMNA), was generally found in EVs from A549 cells, both
145 EV samples were negative for the endoplasmic reticulum-associated protein calnexin (CANX), indicative of good
146 purity of the isolated EV fractions using size-exclusion chromatography (Welsh *et al.* 2024). Due to the similarity
147 between EVs and idEVs in terms of protein content and the lack of apparent antifungal activity, the remainder of
148 the study was performed using spontaneously released EVs to exclude potential artifacts arising from opsonins
149 that are introduced by the opsonization of conidia during the infection process.
150

151 **Transfected A549 epithelial cells properly express and localize tetraspanin-fusion proteins.**

152 After identifying appropriate EV marker proteins, we created plasmids encoding fusion proteins of one of these
153 EV marker proteins, a Nanoluciferase (NLuc), and the fluorescent protein GFP-Spark (green fluorescent protein;
154 GFP). Despite the presence of LMNA in the EVs samples as detected in our proteomic analysis, plasmids
155 encoding for NLuc-GFP-labelled CANX and LMNA fusion proteins were generated as potential controls intended
156 to serve as indicators of the level of introduction of cellular contaminants during EV isolation (**Fig. 2a**). Fusion
157 proteins were each driven by the CMV promoter and constructed to encode an N-terminal NLuc followed by the
158 sequence for GFP and the respective tetraspanin or LMNA at the C-terminal end to not mask the nuclear
159 localization sequence (Anderson *et al.* 2021). Accordingly, since CANX has a signal peptide localized at its N-
160 terminus (Paskevicius *et al.* 2023), the fusion protein was generated to encode N-terminal CANX followed by
161 NLuc and a C-terminal GFP. Purified plasmids were used for the transient transfection of A549 alveolar epithelial
162 cells using a liposome-based approach. Successful transfection and expression of the fusion proteins were
163 verified after 24-hour incubation by fluorescence microscopy and measurement of the luminescence signal in
164 the cell culture supernatant. Generally, GFP fluorescence was detected in cells transfected with all the plasmids.
165 Lactate dehydrogenase (LDH) assays were performed on wild-type and transfected cells to test for cytotoxicity
166 caused by the transfection itself or the specific plasmid preparations. All transfected cells showed slight
167 decreases in viability compared to the non-transfected control cells; however, this was not influenced by the

168 plasmid used (**Sup. Fig. 5a**). In addition, NTA analysis revealed no difference in particle concentration and size
169 distribution of EVs isolated from non-transfected cells compared to transfected cells expressing the tetraspanin
170 fusion proteins of EVs isolated using a commercially available polymer-assisted precipitation method containing
171 polyethylene glycol (PEG) to specifically isolate EVs from the small-scale transfection experiments (**Sup. Fig. 5b**).
172 To observe the subcellular localization of the fusion proteins, transfected cells were subjected to confocal laser
173 scanning microscopy (CLSM). The majority of NLuc-GFP-CD63 fusion proteins accumulated in intracellular,
174 vesicle-like structures and to a lesser extent on the plasma membrane (Levy *et al.* 2020; Mathieu *et al.* 2021; Fan
175 *et al.* 2023) (**Fig. 2b, Sup Fig. 4**). NLuc-GFP-CD81 was localized within the cytoplasm partly accumulating in
176 intracellular vesicles and partly to the plasma membrane (Eppler *et al.* 2011), whereas NLuc-GFP-CD9 fusion
177 proteins were mainly localized to the plasma membrane of the cells (Mathieu *et al.* 2021) (**Fig. 2b, Sup. Fig. 4a**).
178 For the CANX fusion proteins, fluorescent signals were diffusely distributed around the nucleus throughout the
179 cytoplasm (Myhill *et al.* 2008; Jun *et al.* 2014), whereas the signal of the LMNA-fusion proteins were visible
180 around the nucleus as expected (Anderson *et al.* 2021) (**Sup. Fig. 4a**). In addition, luminescence activity was
181 detected in varying intensities in the cell culture supernatants of all transfected cells (**Fig. 2c**). An additional
182 NLuc-GFP fusion protein was tried as a negative control, but this protein was non-specifically localized
183 throughout the whole cell, including the nucleus and extracellular space (Hall *et al.* 2012) (**Sup. Fig. 4b**).
184 Altogether the results confirm the successful production of the fusion proteins, their expected cellular
185 localization, and suggest no major adverse effects of genetic labelling on intracellular trafficking of the
186 tetraspanins.
187

188 **The CD9-, CD81-, and the CD63-fusion proteins are associated with EVs.**

189 In contrast to the tetraspanin fusion proteins, the CANX and LMNA fusion proteins were originally not expected
190 to be sorted into EVs by the transfected cells or secreted into the cell culture supernatant; however,
191 luminescence signals were detected in the supernatants for both LMNA- and to a lesser extent CANX-fusion
192 proteins. Thus, to examine the origin of the measurable luminescence signal, PEG precipitation buffer was added
193 to the conditioned cell culture media and incubated at 4°C followed by low-speed centrifugation, resulting in
194 enrichment of the EVs in the pellet. We hypothesized that the tetraspanin fusion proteins associate with EVs,
195 which in turn would result in an accumulation of the luminescence signal in the EV pellet. In contrast, as shown
196 by our proteomic findings, the CANX and LMNA fusion proteins were expected to be underrepresented or
197 absent in A549 EVs, therefore the signal was hypothesized to mainly accumulate in the EV-depleted supernatant
198 of the sample after EV isolation.

Following EV isolation, NLuc activity was assessed in the resuspended EV pellets as well as in the EV-depleted supernatants. EV isolation using this method resulted in a high luminescence signal deriving from the resuspended EV pellets compared to the EV-depleted supernatants of cells expressing the CD63 and CD9 fusion proteins, indicative of the fusion proteins being associated with EVs (**Fig. 3a**). In the case of the CD81-fusion proteins the enrichment of the signal in the EV fraction was not as prominent and a comparably high signal was also derived from the supposedly EV-depleted supernatant. As expected, little NLuc activity was detected in the EV pellets of cells expressing the CANX and LMNA fusion proteins, but high signals were measurable in the EV-depleted supernatants, suggesting that the respective protein fusions were not associated with EVs.

To further confirm the association of the labelled tetraspanins with EVs, conditioned cell culture media were treated with the non-denaturing detergent Triton X-100 prior to EV isolation. Addition of Triton X-100 leads to the lysis of EVs in the sample (**Sup. Fig. 5c**), releasing EV-associated proteins and molecules into the media and preventing their subsequent precipitation during polymer-assisted EV isolation. Thus, assuming the association of the labelled tetraspanins with EVs, in this setting successful lysis of the EV membrane will result in the luminescence signal deriving from the EV-depleted supernatants instead of the pellets as seen before. Indeed, Triton X-100 treatment led to a clear shift of the luminescence signal from the EV pellet to the EV-depleted supernatant for samples of cells expressing either of the labelled tetraspanins (**Fig. 3b**). This finding further strengthened our hypothesis that these fusion proteins are associated with EVs.

Lastly, transfected cells were treated with the neutral sphingomyelinase inhibitor GW4869 prior to collection of conditioned cell culture media. GW4869 is known to partially block exosome biogenesis (Trajkovic *et al.* 2008; Willms *et al.* 2016; Catalano *et al.* 2020). Assuming that the tetraspanin fusion proteins are associated with EVs, treatment of transfected cells with the inhibitor was expected to decrease the EV-derived luminescence signal in our assays. Cell culture supernatants were collected 6 hours post treatment either with the inhibitor or DMSO as a control and subjected to EV isolation by polymer-assisted precipitation. Subsequently, the resulting EV-enriched pellets were resuspended, and the NLuc signal measured (**Fig. 3c**). Due to high variability of the luminescence signal values between different biological replicates, values were normalised to the untreated controls. Indeed, cell culture media obtained from cells treated with GW4869 revealed a significantly decreased NLuc signal in the EV-pellet (**Fig. 3c**). The decrease in measurable signal correlated positively with increasing concentrations of the inhibitor. In contrast, cells treated with DMSO did not exhibit significantly different NLuc signals compared to the non-treated controls, indicating that the effect is not correlated to DMSO-induced cell toxicity. In addition, LDH assays were performed to verify that the dose-dependent decrease in EV release is not caused by cell death due to the inhibitor itself. A significant decrease of viability was only seen for cells expressing the CD63-fusion proteins when treated with 20 µM GW4869 (**Sup.**

231 Fig. 5d). Thus, the LDH assay indicates that cell death is not solely responsible for the significantly reduced NLuc
232 signal in EV-pellets from transfected cells and supports our previous findings that the fusion proteins are
233 associated with EVs.

234 Collectively, these results suggest that first, the tetraspanin fusion proteins are associated with EVs of
235 A549 epithelial cells, and second, that transfected A549 cells can be used as reporters for the detection and
236 quantification of secreted EVs after their isolation by measurement of luminescence signal.
237

238 GFP-labelled EVs can be visualized using imaging flow cytometry and CLSM.

239 We next wanted to assess whether the isolated EVs from cells expressing the GFP fusion proteins can be
240 visualized. We subjected isolated EVs from transfected and non-transfected cells to imaging flow cytometry. All
241 events that exhibited either a brightfield, side scatter, or GFP signal were captured, including the device internal
242 beads that are important for adjusting the focus. Measurement of the samples revealed a distinct population of
243 events that was only detected in samples expressing the tetraspanin fusion proteins and mostly absent in the
244 sample isolated from non-transfected control cells (Sup. Fig. 5e). Further investigation of this population
245 revealed a high abundance of particles with no brightfield or side scatter signal but a visible GFP signal, likely
246 corresponding to single EVs.

247 Next, to visualise EVs using CLSM, we set up a cell-free system in which EVs isolated from transfected
248 cells were added to *A. fumigatus* germlings. The fungus was cultivated in RPMI in glass-bottom microscopy
249 channel slides that offer limited space for vertical growth and instead force horizontal, planar growth of the
250 hyphae. EV pellets resuspended in small volumes of culture media were added to the fungus and co-incubated
251 for 16 hours in a humidified incubator. After the co-incubation time, samples were directly observed by CLSM.
252 To increase the contrast and resolution, we used the *A. fumigatus* strain AfS150 (Lothe *et al.* 2014), a
253 genetically modified strain expressing the fluorescent protein dTomato within its cytoplasm. Using this strain,
254 overlapping of emission signals was limited and additional washing steps required for most staining protocols
255 that could lead to the loss of EVs were eliminated. CLSM revealed visible green-fluorescent signals in samples
256 treated with EVs isolated from transfected cells expressing any of the labelled tetraspanins compared to
257 untreated control samples (Fig. 4). The visible signal derived from small dot-like to roundish structures, most of
258 which appeared to consist of clusters of EVs. These clusters exhibited varying intensities and sizes with most
259 being far below or around 1000 nm based on the green fluorescence signal, similar to the findings of other
260 groups (Levy *et al.* 2020). Our nanoparticle tracking analysis data of A549 EVs isolated *via* polymer-assisted
261 precipitation with sizes of A549 EVs ranging from approximately 70 – 450 nm (Sup. Fig. 5b) supports our
262 hypothesis that the visible signals partly derive from clumps of EVs. In all cases, labelled EVs were found to co-

263 localise with the fungus, indicating that A549 EVs are indeed able to attach to or associate with *A. fumigatus*
264 hyphae and confirming the value of our system in tracking these interactions.

265 To further verify our findings, we also applied EVs isolated from non-transfected, wild-type A549 cells.
266 To visualise these EVs, we used a novel fluorogenic membrane dye called MemGlow 560 that exhibits minimal
267 fluorescence in its free form. Only the integration into a lipid bilayer leads to high fluorescence signals, which
268 harbours the advantage that isolated EVs can be stained without the need for subsequent washing steps. Since
269 the dye exhibited red fluorescence when integrated into membranes, stained EVs were added to the genetically
270 modified *A. fumigatus* strain AfS35 pJW103 expressing a green-fluorescent mitochondrial tag (Ruf *et al.* 2018)
271 that was also used to assess the antifungal capacity. Conidia were seeded in 8-well microscopy slides and
272 allowed to germinate for 8 hours prior to addition of the EVs. EVs in turn were isolated from cell culture
273 supernatants of A549 cells *via* size-exclusion chromatography, concentrated, and subsequently stained and
274 added to the germlings. After 16 hours of co-incubation, hyphal cell walls were visualised using calcofluor white
275 and the samples were subjected to CLSM. Negative control samples of hyphae treated with the dye diluted in
276 non-EV containing medium displayed no or only minimal red fluorescence signal, showing that the dye is not
277 able to penetrate the fungal cell wall and therefore does not stain the hyphal membrane. In samples treated
278 with stained EVs, several dots of red fluorescence in varying size and intensity accumulating at fungal hyphae
279 were visible (**Fig. 5**). In general, based on the sizes of the red fluorescence signal, EVs stained with the
280 membrane dye appeared to be smaller in size than the genetically labelled EVs, potentially due to reduced
281 clumping and cluster formation after isolation using size-exclusion chromatography.

282 The CLSM images were subsequently subjected to imaging analysis and 3D reconstruction to further
283 investigate the localisation of EVs regarding *A. fumigatus* hyphae (**Fig. 6**). Since labelled EVs were added to the
284 *A. fumigatus* strain AfS150 expressing a cytoplasmic dTomato protein, our 3D models depict the limiting
285 boundaries of the cytoplasm, equivalent to the hyphal membrane. Reconstruction of the EV signal revealed the
286 association of labelled EVs with the hyphal membrane and their internalisation into the hyphal lumen (**Fig. 6 a,b;**
287 **Sup. Video 1**). In the case of MemGlow-stained EVs, experiments were performed using the calcofluor white-
288 stained *A. fumigatus* AfS35 pJW103 strain, with the hyphal cell wall depicted in blue (**Fig. 6c**). Most of the
289 MemGlow signal was localised within the hyphae. Interestingly, the signal appeared to accumulate as a tube-like
290 structure underneath the cell wall, which became even more obvious upon reconstruction of the signal from the
291 GFP-labelled mitochondria within the hyphal lumen. These finding indicate an accumulation of the signal within
292 or associated with the hyphal membrane, consistent with what was observed using the genetically labelled EVs.

293 Finally, we wanted to test whether the genetically labelled EVs can be used to track EVs in our
294 experimental set-up using live cell imaging. As a proof-of-concept we tested EVs isolated from NLuc-GFP-CD9

295 expressing cells using polymer-assisted precipitation. Western blots confirmed the presence of CD9 in EVs
296 isolated from cells expressing either of the labelled tetraspanins or non-transfected control cells. In addition, a
297 clear band corresponding to the NLuc-GFP-CD9 fusion protein was visible for EVs isolated from cells that were
298 transfected with the respective plasmid (**Sup. Fig. 5f**). Isolated EVs were then added to 8-hour-old germlings of
299 the *A. fumigatus* strain AfS150 and imaging was performed over night with a z-stack image being taken every 30
300 minutes (**Sup. Video 2-4**). In the beginning, EVs appeared as small green fluorescent dots that over time started
301 to accumulate at the growing hyphae. Once attached, these EVs still displayed some mobility, but remained
302 attached to the hyphae.

303

304 DISCUSSION

305 PMN-derived EVs were previously found to display antibacterial (Timár *et al.* 2013; Lőrincz Á *et al.* 2015) and
306 antifungal activities (Shopova *et al.* 2020; Rafiq *et al.* 2022) under specific conditions. Here, we attempt to
307 investigate the first steps in the mechanism by which host EVs exert their antifungal functions by exploring the
308 interaction between host cell-derived EVs and *A. fumigatus* hyphae. Our main goal was the visualisation and
309 tracking of these EVs in a live-cell setting; however, EVs are difficult to visualise based on their small size (<1 µm)
310 and heterogeneity. Various methods have been employed in the past such as electron microscopy, staining with
311 dyes, immunofluorescence, and genetic labelling of abundant EV cargo molecules, each with their own
312 advantages and disadvantages (Chuo *et al.* 2018; Verweij *et al.* 2021). In this study, we used two different
313 approaches, lipophilic dyes to stain EV membranes and genetic labelling of abundant EV proteins, which allowed
314 us to detect, visualise, and track genetically labelled EVs in association with *A. fumigatus* hyphae.

315 A549 alveolar epithelial cells served as a tractable model as they are easy to transfect compared to
316 immune cells and have been well-studied during infection with *A. fumigatus* conidia (Paris *et al.* 1997; Zhang *et*
317 *al.* 2005; Amin *et al.* 2014; Jia *et al.* 2014; Zhang *et al.* 2020; Jia *et al.* 2023). We confirmed the successful
318 isolation of EVs and little induction of cell death by LDH release assay consistent with the literature, followed by
319 analysis of their proteomic cargo and antifungal capacity. Interestingly, and in contrast to PMN idEVs (Shopova
320 *et al.* 2020) and PLB-985 idEVs (Rafiq *et al.* 2022), none of the EV populations isolated exhibited antifungal
321 activity in our host cell-free system based on an *A. fumigatus* mitochondrial integrity reporter strain.
322 Consistently, analysis of the proteomic cargo confirmed the absence of any obvious antimicrobial proteins,
323 opposite that of PMN idEVs (Shopova *et al.* 2020). Although the literature reports both activation and repression
324 of inflammatory phenotypes in A549 cells upon co-incubation with *A. fumigatus* conidia (Paris *et al.* 1997; Zhang
325 *et al.* 2005; Amin *et al.* 2014; Jia *et al.* 2014; Escobar *et al.* 2016; Escobar *et al.* 2018; Jia *et al.* 2023), the
326 auxotrophic *A. fumigatus* *pyrG*-deficient strain used here appeared to result in a limited proinflammatory

327 response and may contribute to our observations. This strain provides a fungal stimulus to the cells, while
328 allowing for collection of larger amounts of EVs necessary for proteomics over longer coincubations. It remains a
329 potential complication of these experiments that longer infection time points may result in increased cell stress,
330 low level cell death, and/or alterations to the proteomic cargo of EVs. Fungal proteins were detected
331 inconsistently in the proteomic samples and likely derive from co-isolation of fungal proteins during EV isolation
332 as “contaminants” (Shopova *et al.* 2020; Rafiq *et al.* 2022).

333 Proteomic analysis of EVs confirmed several commonly associated proteins, including the tetraspanins
334 CD63, CD9, and CD81, which are routinely used as EV marker proteins (Lötvall *et al.* 2014; Kowal *et al.* 2016;
335 Lischning *et al.* 2022; Tognoli *et al.* 2023) and to label EVs (Hikita *et al.* 2018; Cashikar *et al.* 2019; Görgens *et al.*
336 2019; Gupta *et al.* 2020). CANX and LMNA were included as negative controls to assess EV purity and the
337 association of the fusion proteins with EVs (Tognoli *et al.* 2023). According to the minimal information for
338 studies of extracellular vesicles (MISEV) guidelines, these proteins are typically absent or underrepresented in
339 EVs; however, they are found in some subtypes of EVs (Théry *et al.* 2018; Welsh *et al.* 2024). Proteomic analysis
340 of wild-type A549 cells indicated that CANX was indeed absent; however, LMNA could be detected in our EV
341 samples. Nonetheless, we created reporters for both control markers and the tetraspanin proteins to have a full
342 repertoire of options for expansion into multiple cell systems in the future. Successful transient overexpression
343 of the panel of NLuc-GFP fusion proteins in A549 cells was confirmed by green fluorescence and luminescence
344 signals in the cell culture media from transfected cells, including those encoding the CANX and LMNA fusion
345 proteins. It is worth noting that overexpression of tetraspanins can impact EV biogenesis and cargo loading, a
346 caveat that must always be considered with any reporter (Strohmeier *et al.* 2021), and subsequently future
347 studies will be required to more finely localize our new reporters in particular EV subpopulations. Nonetheless,
348 we observed release of all the fusion proteins into the cell culture supernatant in accordance with previous
349 observations (Cashikar *et al.* 2019; Gupta *et al.* 2020); however, isolation of EVs from cell culture supernatants
350 revealed that the CANX and LMNA fusion proteins were not associated with the EV fraction, as initially expected.
351 In addition, lysis of EVs in cell culture supernatants prior to their isolation demonstrated the association of the
352 fusion proteins with A549 EVs. As an orthogonal approach, we confirmed a dose-dependent decrease of signal in
353 the EV-containing fraction upon treatment of transfected cells with the neutral sphingomyelinase inhibitor
354 GW4869 known to reduce EV biogenesis via the ESCRT-independent exosome biogenesis pathway (Trajkovic *et*
355 *al.* 2008; Kulshreshtha *et al.* 2013; Essandoh *et al.* 2015). We used high levels of GW4869 as described in the
356 literature and did observe some LDH release indicative of cell death in this assay, yet overall the result appears
357 to imply that the reporters decreased along with EV numbers. The successful generation of the reporter panel
358 allowed for detection and relative quantification of EVs by luminescence signal, while simultaneously enabling

359 their visualisation within the cells for subcellular localisation and transfection efficiency, simplifying the overall
360 workflow associated with such a reporter assay.

361 Imaging flow cytometry on the tetraspanin reporters from isolated EVs detected events of green
362 fluorescent particles with minimal to no visible brightfield or side scatter signal. The absence of the brightfield
363 signal is indicative of particles with sizes below the optical resolution limit of the device of 200 nm, consistent
364 with sizes corresponding to small EVs (Headland *et al.* 2014; Abels *et al.* 2016) and in accordance with previous
365 studies investigating GFP-labelled EVs from THP-1 monocytes (Görgens *et al.* 2019) and HEK293 cells
366 (Jurgielewicz *et al.* 2020), as well as immuno-labelled EVs (Ricklefs *et al.* 2019). Using CLSM, EVs appeared as
367 small, green fluorescent dots of varying size and intensity similar to the findings of previous studies using
368 genetically labelled fluorescent EVs (Corso *et al.* 2019) and immunolabelled or stained EVs (Mondal *et al.* 2019).
369 Importantly, part of the visible signal was clearly associated with fungal hyphae, indicating that A549 EVs can
370 interact with *A. fumigatus*. This co-localisation was seen for all EVs regardless of the labelled tetraspanin
371 expressed, hinting towards a nonspecific interaction. We verified these findings using MemGlow stained A549
372 EVs from non-transfected cells. While the dye alone was almost completely unable to penetrate the cell wall of
373 *A. fumigatus* hyphae, addition of stained EVs led to accumulation of co-localised signal with *A. fumigatus* hyphae
374 as dot-like structures, similar to the EVs labelled with reporter proteins. One major difference observed between
375 the two experiments was the amount of EVs binding to the hyphae, which is likely caused by the higher
376 proportion of labelled EVs using the MemGlow approach. These EVs were isolated via size-exclusion
377 chromatography from a large number of cells. Even though this isolation method led to a dilution of the sample
378 (Welsh *et al.* 2024), the total amount of labelled EVs in the final sample was likely higher than from the low-
379 efficiency transfection experiments. While the lipophilic dye can stain many subsets of EVs, it was previously
380 shown that the tetraspanins CD63, CD81, and CD9 distribute heterogeneously across EV subsets (Ricklefs *et al.*
381 2019; Han *et al.* 2021), resulting in even fewer labelled versus stained EVs. Different tagging approaches can
382 alter the properties and fate of EVs, so it is recommended to use different labelling methods when studying EVs
383 (Loconte *et al.* 2023). Here, the similar outcomes of the two strategies employed provides confirmatory
384 evidence for the use of either our tetraspanin fusion proteins or MemGlow dye as the situation necessitates, but
385 certainly orthogonal support is required for each specific experiment.

386 Lastly, imaging analysis and 3D-reconstruction of the microscopy images indicated that both labelled
387 and stained A549 EVs are attached and partly internalised by *A. fumigatus* hyphae. This was an interesting
388 finding that brings us one step further into understanding how EVs can exert effects on the fungus. First, it is
389 now clear that the interaction of EVs with fungal hyphae is not limited to EVs produced by infected cells, but
390 instead a more widespread phenomena, potentially even serving as a food source for the fungus in some cases.

391 It is also likely that the interaction of EVs alone cannot explain the antifungal activity previously observed for
392 PMN (Shopova *et al.* 2020) and PLB-985 idEVs (Rafiq *et al.* 2022). The mechanisms behind the attachment of EVs
393 to hyphae and their subsequent internalisation remain unclear and will be objectives of future studies, but
394 based on their ability to fuse with membranes (Morandi *et al.* 2022), one hypothesis could be that EVs are able
395 to pass the cell wall, either actively or passively, followed by fusion of the EV membrane with the hyphal
396 membrane to release cargo. A more active form of fungal cell-induced endocytosis also remains possible. In
397 mammalian cells, evidence suggests that EVs can be taken up into the endosomal/lysosomal pathway via
398 endocytosis and that the release of EV cargo within recipient cells is often pH-dependent (Mulcahy *et al.* 2014;
399 Bonsergent *et al.* 2021). More generally, successful uptake and cargo delivery of host cell EVs by fungi was
400 previously demonstrated in plant-fungal-interactions (Cai *et al.* 2018; Wang *et al.* 2024).

401 In conclusion, our knowledge of host cell-derived EVs in immunity to *A. fumigatus* is still very limited.
402 With these findings, we can confirm that EVs produced by naive human alveolar epithelial cells robustly interact
403 with *A. fumigatus* hyphae, but fail to trigger an antifungal response. In the future, this methodological proof-of-
404 principle using genetic labelling of A549 cell-derived EVs will serve as a platform to be expanded to other cell
405 types as well as other target proteins.

406

407 MATERIALS AND METHODS

408 Culture conditions of microorganisms.

409 *A. fumigatus* conidia (**Sup. Table 1**) were plated on malt agar (Sigma Aldrich) and incubated at 37°C. On day five,
410 conidia were collected from plates by adding 10 mL of sterile ultrapure water (dH₂O) to the plate and scraping
411 the conidia off the agar using a disposable T-shaped scraper. The conidia-water suspension was filtered through
412 a 30 µm cell strainer (MACS, Miltenyi Biotec GmbH) for the removal of mycelium. Conidia were washed by
413 centrifugation at 1,800 × g and 4°C for 5 min followed by removal of the supernatant and resuspension in sterile
414 dH₂O. Conidia were stored at 4°C for no longer than a week before use.

415

416 Cell culture.

417 A549 epithelial cells were cultivated in Kaighn's Modification of Ham's F-12 (F-12K) medium (Gibco)
418 supplemented with 10% (v/v) artificial FCS (FetalClone III; Cytiva) and penicillin/streptomycin to a final
419 concentration of 1%. Cells were seeded into T25 or T75 cell culture flasks at concentrations of 2×10⁵ and 3×10⁵,
420 or 6×10⁵ and 1×10⁶ cells per flask and passaged after four and three days, respectively. Spent media was
421 removed by aspiration and cells were washed using prewarmed Ca²⁺/Mg²⁺-free PBS (Gibco). Cells were detached
422 from the cell culture flasks through the addition of trypsin (Thermo Fisher Scientific) and were subsequently

423 incubated at 37°C with 5% (v/v) CO₂ for 5 minutes followed by gentle tapping of the culture flask to assure the
424 detachment of all cells. Trypsinisation was stopped by the addition of FCS-containing F-12K medium and cells
425 were transferred to a fresh tube. Cell concentrations were determined using the Luna cell counter and cells
426 were seeded into a new culture flask containing pre-warmed media for culturing or into plates as needed for the
427 respective experiments. Seeded cells were incubated at 37°C and 5% (v/v) CO₂. If required, cells were seeded in
428 EV-depleted medium consisting of F-12K medium supplemented with 1% (v/v) EV-depleted FCS ("exosome-free
429 serum", Life Technologies GmbH).

430

431 **Infection of cells with *A. fumigatus*.**

432 A549 epithelial cells were seeded into 15 cm culture dishes at concentrations of 2×10^7 cells/dish in EV-depleted
433 medium on the day prior to infection and incubated at 37°C and 5% (v/v) CO₂. On the day of infection, fungal
434 conidia suspensions were washed by centrifugation with $1,800 \times g$ at 4°C for 5 minutes and the pellet was
435 resuspended in 900 µL sterile PBS. Conidia were opsonised by the addition of 100 µL normal human serum
436 followed by incubation at 37°C and centrifugation with 350 rpm for 30 minutes. Subsequently, the conidia were
437 washed three times with sterile PBS and the concentration determined using a Thoma haemocytometer. Cells
438 were washed using PBS and fresh pre-warmed EV-depleted medium in addition to opsonised fungal conidia to a
439 multiplicity of infection (MOI) of 5, was added to the cells. Control experiments were treated with medium
440 without fungal conidia. The plates were incubated at 37°C and 5% (v/v) CO₂ for 8 or 24 hours before EV isolation
441 by size-exclusion chromatography.

442

443 **EV isolation by size-exclusion chromatography (SEC).**

444 Conditioned cell culture medium was collected from cells and centrifuged at $3000 \times g$ and 4°C for 15 minutes,
445 filtered through a 0.22 µm syringe filter (Carl Roth) and concentrated using Amicon Ultra-15 centrifugal filters
446 (molecular weight cut-off: 100 kDa; Merck) by centrifugation at 4°C and $3,220 \times g$. First, as a pre-experiment to
447 test for successful isolation of EVs samples were loaded onto pre-washed qEV 70 nm size-exclusion
448 chromatography columns (Izon). Samples were isolated using Ca²⁺/Mg²⁺-free PBS (Gibco). The first 2 mL of flow
449 through corresponding to fractions 1-4 were collected followed by the collection of single fractions of 0.5 mL
450 each until fraction 12. All of these samples were subjected to NTA analysis to check for particle size and
451 concentration in the different fractions. Finally, throughout the remaining study, concentrated samples were
452 loaded onto pre-washed qEV 70 nm size-exclusion chromatography columns (Izon) and isolated using Ca²⁺/Mg²⁺-
453 free PBS (Gibco). Based on the results from the pre-experiment and in accordance with the manufacturer's
454 protocol, the first 3 mL corresponding to fractions 1-6 was considered as void volume and discarded, followed by

455 collection of the 1.5 mL EV-containing fractions 7-9. EVs were used for nanoparticle tracking analysis (NTA) or in
456 case of sample preparation for proteomic analysis, western blots, or treatment of fungal hyphae, further
457 concentrated using 10 kDa cut-off Amicon Ultra-0.5 ml filters (Merck) and stored at -20°C until usage.

458

459 **Nanoparticle tracking analysis (NTA).**

460 Particle concentrations and size distributions of purified EV samples were assessed by NTA using a
461 NanoSight 300 device (Malvern Instruments Ltd.). Samples were measured at ambient room temperature at a
462 constant flow rate of 20 with the camera level set to 14 and the detection threshold to 4. For each sample,
463 either three videos of 45 second each or five videos of 60 seconds each were obtained as indicated and
464 subsequently analyzed with the NTA 3.2.16 software.

465

466 **Proteomic analysis of isolated EVs.**

467 EVs were isolated by size-exclusion chromatography from conditioned medium of uninfected A549 cells and
468 cells infected with the *A. fumigatus* *pyrG* strain after 24 hours of incubation at 37°C and 5% (v/v) CO₂ in EV-
469 depleted medium. Preparation of protein samples from SEC isolated EV samples, LC-MS/MS analysis, and
470 database search and analysis were performed as described before (Rafiq et al. 2022), except for the following
471 changes: LC-MS/MS analysis was performed on a Q Exactive Plus mass spectrometer (Thermo Fisher Scientific).
472 Gradient elution was as follows: 0-5 min at 4% B, 30 min at 7% B, 60 min at 10% B, 100 min at 15% B, 140 min at
473 25% B, 180 min at 45% B, 200 min at 65% B, 210-215 min at 96% B, and 215.1-240 min at 4% B. The instrument
474 was operated in full MS/data-dependent MS2 (Top10) mode. Precursor ions were monitored at a resolution of
475 140,000 FWHM (full width at half maximum). After higher-energy collisional dissociation (HCD) fragmentation at
476 30% normalized collision energy (NCE), MS2 ions were scanned at 17,500 FWHM and a maximum injection time
477 of 120 ms. Dynamic exclusion of precursor ions was set to 30 s. Tandem mass spectra were searched against the
478 UniProt database of *Homo sapiens* (<https://www.uniprot.org/proteomes/UP000005640>; 21 March 2019) and
479 *Aspergillus fumigatus* (<https://www.uniprot.org/proteomes/UP000002530>; 21 March 2019) using Proteome
480 Discoverer (PD) 2.2 (Thermo) and the algorithms of Mascot 2.4.1 (Matrix Science), Sequest HT (version of
481 PD2.2), and MS Amanda 2.0.

482

483 **Assessment of the antifungal capacity of EVs.**

484 To assess the antifungal capacity of EVs, 1×10⁴ conidia of the *A. fumigatus* AfS35/pJW103 strain (Ruf et al. 2018)
485 were seeded into an 8-well microscopy slide (μ-Slide 8 Well Polymer Coverslip, Ibidi) in 200 μL Roswell Park
486 Memorial Institute (RPMI) medium (Gibco) and allowed to germinate for 8 hours at 37°C and 5% CO₂. EVs were

487 isolated from uninfected or infected A549 cells after 8 hours via SEC and added to the germlings followed by
488 incubation over night at the above-mentioned conditions. On the following day fungal hyphae were stained with
489 Calcofluor white, subjected to CLSM imaging using a Zeiss LSM 780 confocal microscope, and evaluated with the
490 Zen software (Carl Zeiss).

491

492 **Generation of the plasmids encoding fusion proteins and transformation of *Escherichia coli*.**

493 DNA fragments for Gibson cloning were prepared as follows: DNA fragments were amplified from an
494 appropriate template by PCR using a primer pair (**Sup. Table 2, 3**), and PCR fragments were purified using the
495 GeneJet PCR Purification kit (Thermo Fisher Scientific). The plasmid backbone was prepared by restriction
496 digestion of the circular plasmid pNLF1-N (Promega) with *EcoRV* or *EcoRI* for C- or N-terminal cloning,
497 respectively. Gibson cloning was performed using the NEBuilder HiFi DNA Assembly Master Mix (New England
498 Biolabs) according to the manufacturer's protocol using the primers described in **Sup. Table 3**, and the reaction
499 was subsequently used for the transformation of chemically competent *E. coli* cells (NEB® Turbo Competent *E.*
500 *coli*, New England Biolabs). The final constructs are shown in **Fig. 2**, where each reporter construct is driven by a
501 CMV promoter.

502

503 **Transient transfection of A549 epithelial cells using Lipofectamine 3000®.**

504 Transfection using Lipofectamine® 3000 (Invitrogen) was performed in 24-well plates according to the
505 manufacturer's instructions. Briefly, on the day before transfection, A549 epithelial cells were seeded into a 24-
506 well plate at densities of 1×10^5 cells/well and incubated at 37°C and 5% (v/v) CO₂ for 20 hours to allow the cells
507 to attach. The transfection solution per well was prepared as follows: In two separate reactions, 1.5 µL
508 Lipofectamine® and 1 µL P3000® reagent, together with 500 ng of the desired plasmid DNA for transfection,
509 were diluted in 25 µL F12-K medium (Gibco). The contents of both tubes were combined to yield the
510 transfection reaction, which was incubated at room temperature for 10-15 minutes. In the meantime, the cells
511 were washed using pre-warmed PBS and 450 µL pure F-12K medium was added to each well. 50 µL of the
512 transfection reaction was added to the wells in a dropwise manner, followed by gentle swirling of the plate to
513 ensure an equal distribution. The plates were incubated at 37°C and 5% (v/v) CO₂. 22 hours post transfection,
514 cells were washed with pre-warmed PBS and incubated in 1 mL EV-depleted medium. The cells were incubated
515 under the above-mentioned conditions for the appropriate times depending on the following experiments. For
516 microscopy, cells were seeded on glass cover slips prior to transfection. On the day of microscopy, cell
517 membranes were stained with Cell Mask Deep Red (Invitrogen) for 10 minutes at 37°C and nuclei with DAPI-
518 containing mounting medium (Roti-Mount FluorCare DAPI; Carl Roth).

519

520 **Assessment of cell viability.**

521 To assess cell viability, lactate dehydrogenase (LDH) assays were performed using a commercially available
522 fluorometric LDH assay kit (Abcam) according to the manufacturer's protocol. Briefly, culture medium was
523 collected from transfected and non-transfected control cells after 24 hours, centrifuged at 10,000 × g at 4°C for
524 5 min, and supernatants were transferred to fresh microcentrifuge tubes. Cell lysates were also prepared from
525 untreated cells by scraping and resuspension in assay buffer to assess the maximum LDH amount required for
526 the calculation of cell viability. Cell supernatants and lysates were kept on ice and either directly used for
527 measurement or snap frozen and stored at -20°C until the following day. Standards and reagents were prepared
528 freshly for every measurement. Samples and standards were diluted in assay buffer and after addition of the
529 assay reagent, fluorescence signal was measured in kinetic mode at 37°C at excitation/emission 535±15
530 nm/587±20 nm every 2 min for a total of 30 min using a plate reader M200 PRO plate reader (Tecan group Ltd.).
531 Viability was calculated according to the method in the protocol.

532

533 **GW4869 treatment of cells.**

534 GW4869 (Sigma Aldrich) was resuspended in DMSO to a final concentration of 10 mM. This oversaturated stock
535 solution was used for further dilution in cell culture media as previously described in the literature (Józefowski
536 *et al.* 2010; Essandoh *et al.* 2015; Slivinschi *et al.* 2022). Transfected A549 cells were washed with PBS 22 hours
537 post transfection and incubated in 1 mL F-12K medium containing 1% (v/v) EV-depleted FCS and the appropriate
538 amount of GW4869 to obtain final concentrations of 20 µM and 40 µM. Negative controls were incubated in
539 culture media without the addition of GW4869 while DMSO controls were incubated in culture media containing
540 the identical volume of DMSO as 40 µM GW4869 stock solution in the treated samples. Since DMSO is itself
541 toxic, the highest volume of DMSO without the inhibitor was used as a control to ensure potential outcomes
542 were not due to DMSO toxicity. Cells were incubated at 37°C and 5% (v/v) CO₂ for 6 hours. All conditions were
543 carried out as 3 technical replicates per biological replicate.

544

545 **EV isolation using polymer-assisted precipitation.**

546 Conditioned cell culture medium was collected from transfected cells after 6 or 24 hours, depending on the
547 experiment, and centrifuged at 3,000 × g at 4°C for 15 minutes to pellet dead cells and debris. For EV isolation
548 500 µL of the supernatants were transferred to fresh microcentrifuge tubes and the miRCURY® Exosome
549 Cell/Urine/CSF kit (Qiagen) was used according to the manufacturer's protocol. Briefly, 200 µL of precipitation
550 buffer B was added to the supernatant and mixed thoroughly by vortexing. The samples were incubated at 4°C

551 for one hour followed by centrifugation with $10,000 \times g$ at room temperature for 30 minutes to pellet EVs. The
552 supernatants were completely removed by gentle pipetting and stored for NLuc measurement when required.
553 The remaining EV pellet was resuspended in filtered PBS. Samples were used directly for NTA analysis,
554 measurement of the NLuc signal, or snap frozen in liquid nitrogen and stored at -80°C until usage.

555

556 **Western blot analysis.**

557 Cell lysates of transfected and non-transfected control cells were prepared by scraping and resuspension in
558 radioimmunoprecipitation assay (RIPA) buffer (Thermo Fisher Scientific) supplemented with 1X protease
559 inhibitor (Roche). EV lysates were prepared by addition of RIPA buffer and 1X protease inhibitor to isolated EVs.
560 Protein concentrations were determined using the Qubit 4 Fluorometer with the Qubit Protein Broad Range
561 Assay Kit (Thermo Fisher). 15 or 40 µg of protein were mixed with 1x NuPAGE LDS sample buffer (Thermo Fisher)
562 and incubated at 95°C for 10 minutes. Protein preparations were loaded onto NuPAGE 4-12% Bis Tris gels
563 (Invitrogen) for separation followed by blotting onto a 0.2 µm pore size PVDF membrane (Invitrogen) in an iBlot
564 3 Western Blot Transfer System device (Thermo Fisher Scientific) using the pre-set settings for broad-range
565 protein transfer. Membranes were blocked with 5% (w/v) milk powder in PBS with 0.5% (v/v) Tween20 for 1
566 hour at room temperature and subsequently incubated with the respective primary antibodies diluted in 5%
567 (w/v) milk powder in PBS with 0.5% (v/v) Tween20 at 4°C overnight. The following day, membranes were
568 washed three times with PBS with 0.5% (v/v) Tween20 for 10 minutes before incubation with the secondary
569 antibody for 1 hour at room temperature. Washing steps were repeated as described above and membranes
570 were developed by addition of 1-Step Ultra TMB Blotting Solution (Pierce, Thermo Fisher Scientific). Anti-CD9
571 (Abcam, AB236630), Anti-CANX (Abcam, AB22595), Anti-CD81 (Abcam, AB109201), Anti-CD63 (Abcam,
572 AB271286 and AB134045) Anti-Lamin A (Cell Signaling Technology, 133A2), and Anti-ALIX (Cell Signaling
573 Technology, 3A9) were used as primary antibodies. The secondary antibodies used were goat Anti-Rabbit IgG
574 H&L (HRP) (Abcam, AB6721) and horse Anti-mouse IgG (HRP) (Cell Signaling Technology, 7076S).

575

576 **Lysis of EVs.**

577 Conditioned cell culture media was collected from transfected cells after 24 hours and centrifuged with $3,000 \times g$
578 at 4°C for 15 minutes to pellet dead cells and debris. 400 µL of the supernatants were treated with 10% (v/v)
579 Triton-X 100 at a final concentration of 0.2% (v/v) for 15 minutes at room temperature. During this time samples
580 were inverted and vortexed regularly. After incubation, 300 µL of the sample was transferred to a new
581 microcentrifuge tube for EV isolation using the miRCURY® Exosome Cell/Urine/CSF kit (Qiagen) as described
earlier.

583

584 **Measurement of the NLuc activity.**

585 NLuc activity was measured from cell culture media and isolated EVs from transfected cells using the NanoGlo®
586 Luciferase Assay System (Promega GmbH, Germany) according to the manufacturer's protocol with slight
587 modifications. Briefly, 10 µL of sample and 15 µL of dH₂O were pipetted into the wells of a white, flat-bottom 96
588 well plate. The assay reagent was prepared by mixing 2 µL of NanoGlo® Luciferase Assay Substrate with 100 µL
589 of NanoGlo® Luciferase Assay Buffer. 25 µL of the reagent was added to each well and mixed on a plate shaker.
590 After 3 minutes of incubation at room temperature, the NLuc activity was examined by measurement of the
591 luminescence signal using an Infinite M200 PRO plate reader (Tecan group Ltd.).

592

593 **Imaging flow cytometry.**

594 Imaging flow cytometry of isolated EVs from transfected cells was performed using an Amnis® ImageStream[®]
595 MKII device. Briefly, cells were transfected and washed as described above. Conditioned cell culture media from
596 2.4×10⁶ cells per condition and construct was collected after 24 hours and EVs were isolated via polymer-
597 assisted precipitation. Isolated EVs were resuspended in 100 µL 0.22 µm filtered Ca²⁺/Mg²⁺-free PBS (Gibco) and
598 stored at -20°C. EVs from non-transfected cells served as negative control. The device was calibrated before
599 each use. The magnification was set to 60x, flow speed to low, and sensitivity to high. Brightfield images were
600 obtained in channel 4 and 10, green fluorescence (488 nm) in channel 2, and the side scatter (SSC, 785 nm) in
601 channel 6. Laser intensities were adjusted to 120 mW for the green laser and 5.16 mW for the SSC. All events
602 including the device-internal speed beads were acquired, and the number of events was set to 20,000 per
603 sample. Analysis of the data was performed using the Image Data Exploration and Analysis Software (IDEAS®,
604 Amnis), version 6.2. Briefly, EVs were considered to appear as particles without a visible brightfield signal, hence
605 the area of the brightfield signal was plotted against the intensity of the brightfield signal. This allowed us to
606 exclude all events with a brightfield signal from the sample population and included the device-internal
607 SpeedBeads as well as clumps of cellular material. Subsequently, to visualise GFP-labelled EVs, the signal
608 intensity of the GFP channel was plotted against the normalized frequency of the occurring events. Within these
609 plots a cut-off was set at 1×10³ for particles to be assessed as GFP-positive while particles with GFP intensity
610 signals below this threshold were considered to be GFP-negative.

611

612 **Treatment of fungal hyphae with reporter gene-expressing EVs.**

613 *A. fumigatus* conidia were washed by centrifugation at 1800 × g and 4°C for 5 minutes, resuspended in sterile
614 dH₂O and the concentration was determined using a Thoma haemocytometer. 2×10⁴ spores in 300 µL RPMI

615 were pipetted into a glass bottom channel slide (μ -Slide Luer, 0.6, Glass Bottom, Ibidi) and incubated at 37°C and
616 5% (v/v) CO₂ for 8 hours or overnight to allow for germination or the formation of hyphae, respectively. For EV
617 treatment, 150 μ L of the spent media was removed from the channel slide and isolated EVs from 2.4×10^6
618 transfected cells resuspended in 150 μ L fresh RPMI were added to the hyphae. Due to challenges in quantifying
619 the exact number of tagged extracellular vesicles, we can only approximate the number of particles delivered to
620 *A. fumigatus* based on our transfection efficiency and quantification of total particles by NTA. We used a ratio of
621 roughly 250 to 1 for cells to fungus, but as we expect only 10-15% of cells to be transfected and many EVs to be
622 lost during isolation, we expect to have only a minor excess of EVs to fungal hyphae in the actual experiment. To
623 achieve a more homogenous distribution of the EVs within the channel slide, 150 μ L media was removed from
624 the channel opening on the right-side and re-added into the left-side opening of the channel. This step was
625 repeated 5 times for every sample. Negative controls were treated similarly but with cell culture media lacking
626 labelled EVs. Channel slides were then incubated at 37°C and 5% (v/v) CO₂ for a total of 24 hours prior to being
627 subjected to CLSM imaging using a Zeiss LSM 780 confocal microscope with a 63x oil immersion objective lens
628 with a numerical aperture of 1.40, a refractive index of n=1.518, and voxel size of 188x188x850 nm. Evaluation
629 of the images was performed using the Zen software (Carl Zeiss). Live cell imaging was performed by addition of
630 labelled EVs to *A. fumigatus* germlings as described above. Samples were incubated in the incubation chamber
631 of the Zeiss LSM 780 confocal microscope at 37°C with 5% (v/v) CO₂. A pre-set z-stack of images was captured
632 every 30 minutes using the 63x oil immersion objective lens with a numerical aperture of 1.40 and a refractive
633 index of n=1.518.

634

635 **Treatment of fungal hyphae with stained EVs.**

636 1×10^4 conidia in 200 μ L RPMI were seeded into the chambers of an 8-well microscopy slide (μ -Slide 8 Well
637 Polymer Coverslip, Ibidi) and incubated at 37°C and 5% (v/v) CO₂ for 8 hours to allow for germination. After the
638 incubation time, MemGlow 560 (Cytoskeleton) was used to stain concentrated EV samples isolated from 1×10^7
639 non-transfected A549 cells per sample by SEC. More precisely, MemGlow 560 was added to the sample to reach
640 a final concentration of 200 nM and the sample was directly mixed thoroughly by vortexing and immediately
641 thereafter added into the media of the respective wells of the microscopy slide. The samples were then mixed
642 by carefully pipetting up and down and the microscopy slide was returned to 37°C and 5% (v/v) CO₂ for 16 hours.
643 Control samples were treated with MemGlow 560 diluted in unconditioned media to a final concentration of
644 200 nM. The following day hyphae were stained with Calcofluor white, subjected to CLSM imaging using a Zeiss
645 LSM 780 confocal microscope with a 63x oil immersion objective lens with a numerical aperture of 1.40, a

646 refractive index of n=1.518, and a voxel size of 132x132x400 nm. Images were evaluated with the Zen software
647 (Carl Zeiss).

648

649 **Imaging Analysis.**

650 Three-dimensional images were provided in the CZI (Carl Zeiss Image) native microscopy format. The main steps
651 of the image processing and quantification are summarized in **Sup. Fig 6**. At first, the raw 3D images were
652 deconvolved using the Huygens Professional software (SVI, Hilversum, The Netherlands, <https://www.svi.nl>),
653 applying a measured point spread function detected from the actual samples using 170 nm fluorescent plastic
654 beads with excitation and emission wavelengths that matched those of the biological samples. The deconvolved
655 images were saved in TIFF format and proceeded to Imaris (Bitplane, Zürich, Switzerland,
656 <https://www.bitplane.com>) for further analysis. Here Imaris 10.2 was applied, where we used batch processing
657 scripts to segment all components, including the hyphal wall, EVs, and the mitochondria. Each processed image
658 was manually checked for possible segmentation errors. The hyphal segmentation revealed the actual wall
659 boundaries, allowing the precise measurement and visualisation of the EVs' spatial position relative to the
660 hyphal cell wall. Furthermore, EVs were quantified after segmentation as Spots objects in Imaris, where they
661 were allowed to have various radii, in order to account for the possible presence of unresolvable small EV
662 clusters (**Fig. 6**).

663

664 **Data Availability.**

665 The mass spectrometry proteomics data have been deposited to the ProteomeXchange Consortium via the
666 PRIDE (Perez-Riverol *et al.* 2022) partner repository with the dataset identifier PXD050398.

667

668 **Statistical Analysis.**

669 GraphPad Prism 10.1.0 software was used for data plotting and statistical analysis. The Student's t test was used
670 for the comparison of two groups and one-way or two-way ANOVA for the comparison of multiple groups. All
671 bar graphs are depicted with standard deviation of the mean (SEM). Significance was defined as follows: *,
672 $p = <0.05$; **, $p = <0.01$; ***, $p = <0.001$; ns, not significant.

673

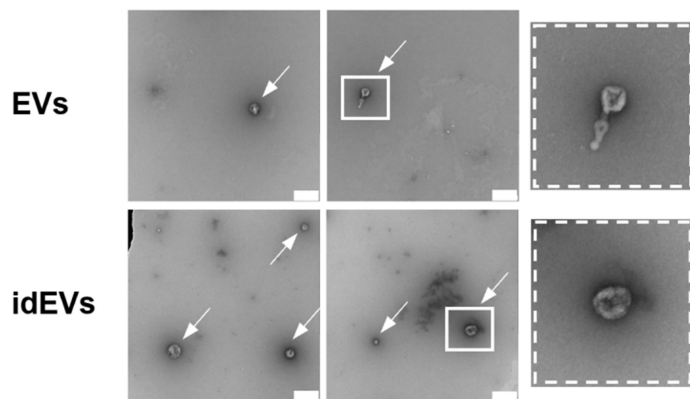
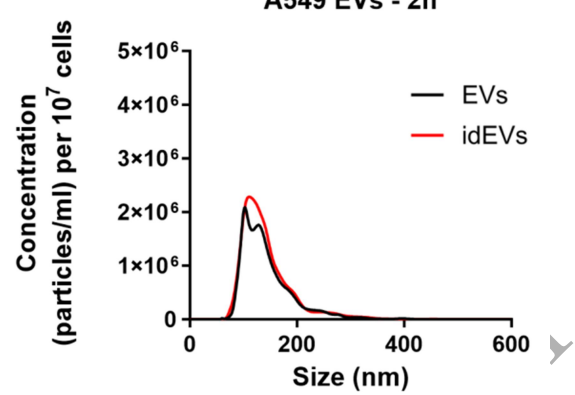
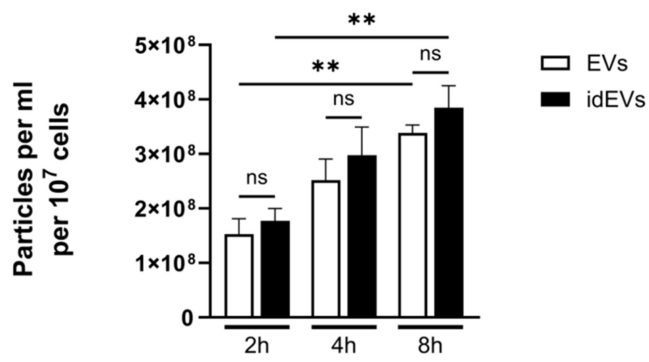
674 **ACKNOWLEDGEMENTS**

675 We thank Johannes Wagener for providing the *A. fumigatus* mitochondrial-GFP strain and Maximilian Knott for
676 excellent technical support. This work was supported by the Deutsche Forschungsgemeinschaft (DFG)-funded
677 Collaborative Research Center/Transregio 124 FungiNet (project number 210879364, projects A1, B4 and Z2),

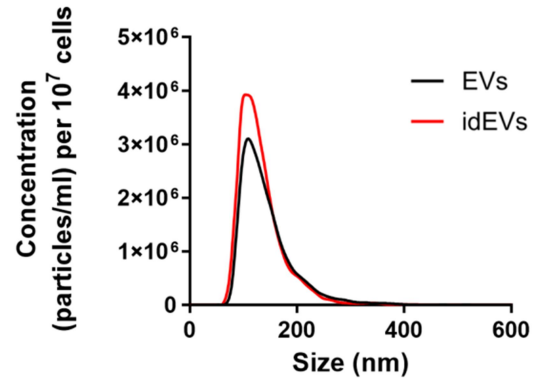
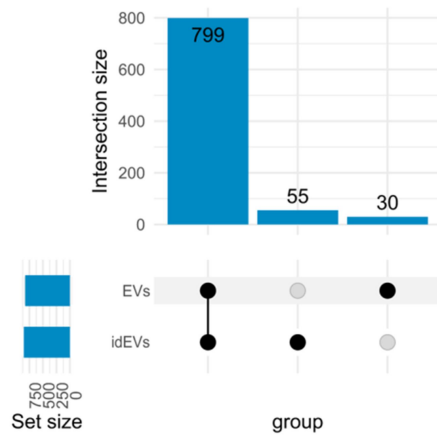
678 the Cluster of Excellence *Balance of the Microverse* under Germany's Excellence Strategy (EXC 2051; project ID
679 390713860, and the DFG-funded Collaborative Research Centre PolyTarget (Project-ID: 316213987 – SFB 1278;
680 project Z01). M.G.B. was supported by the Federal Ministry for Education and Research (BMBF:
681 <https://www.bmbf.de/>), Germany, Project FKZ 01K12012 "RFIN – RNA-Biologie von Pilzinfektionen." The funders
682 had no role in the study design, data collection and analysis, decision to publish, or preparation of the
683 manuscript. The authors declare no conflicts of interest.

684

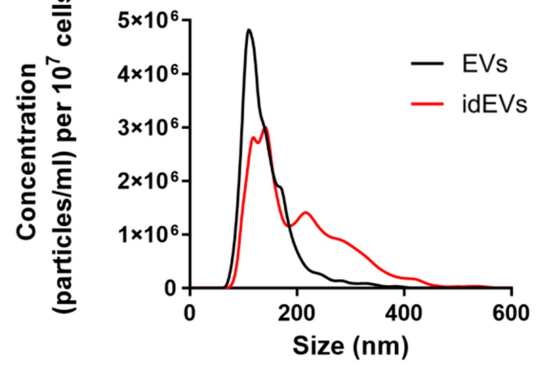
685

A**C****B**

Concentration (particles/ml) per 10^7 cells

A549 EVs - 4h**D**

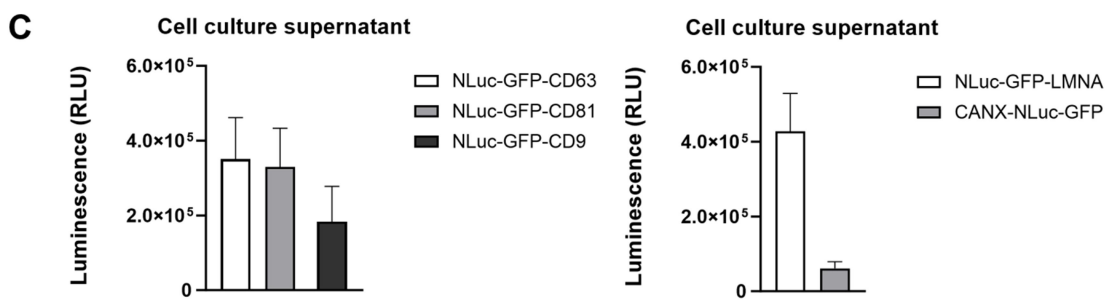
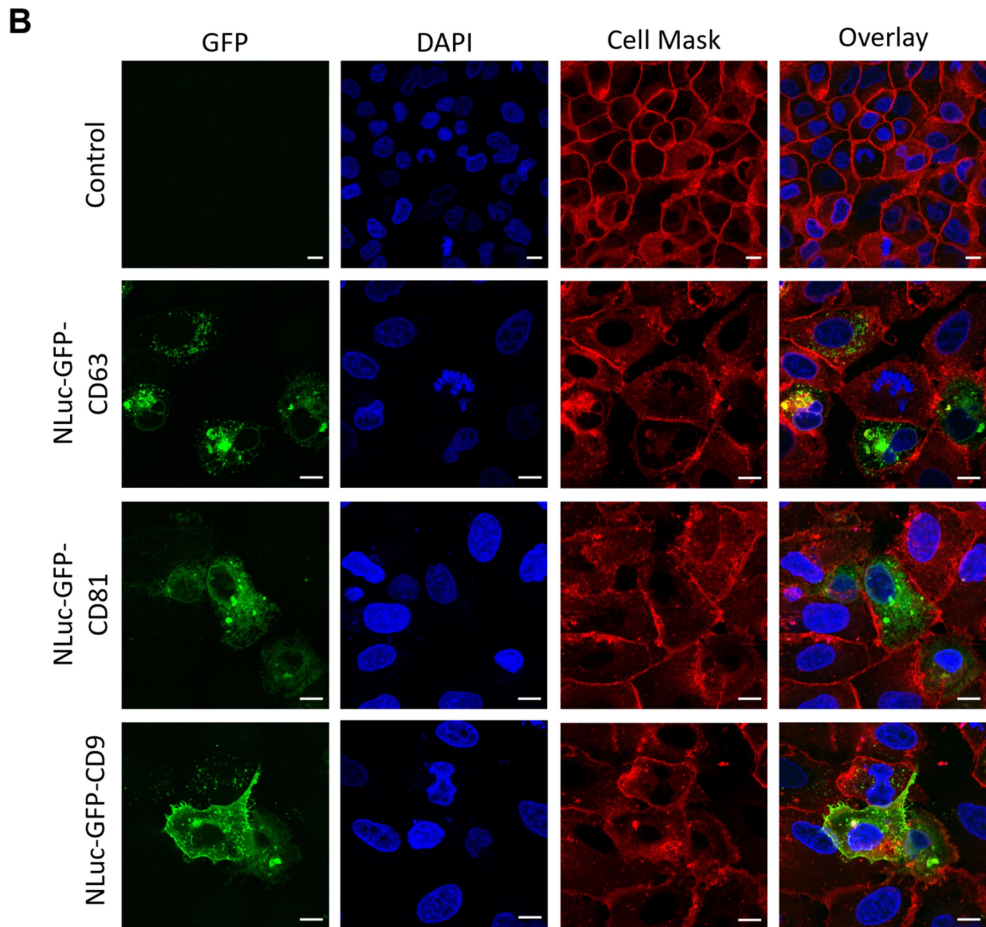
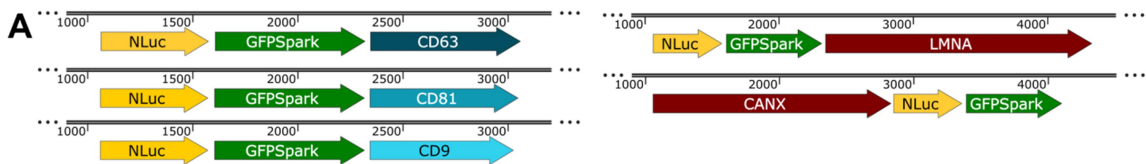
Concentration (particles/ml) per 10^7 cells

A549 EVs - 8h

689 **A)** Representative transmission electron microscopy images of A549 EVs (arrows). Upper lane: EVs were isolated
 690 from cell culture supernatants of untreated cells (spontaneously produced EVs; EVs). Lower lane: EVs were
 691 isolated from cell culture supernatants of cells previously infected with *A. fumigatus* conidia (*A. fumigatus*-

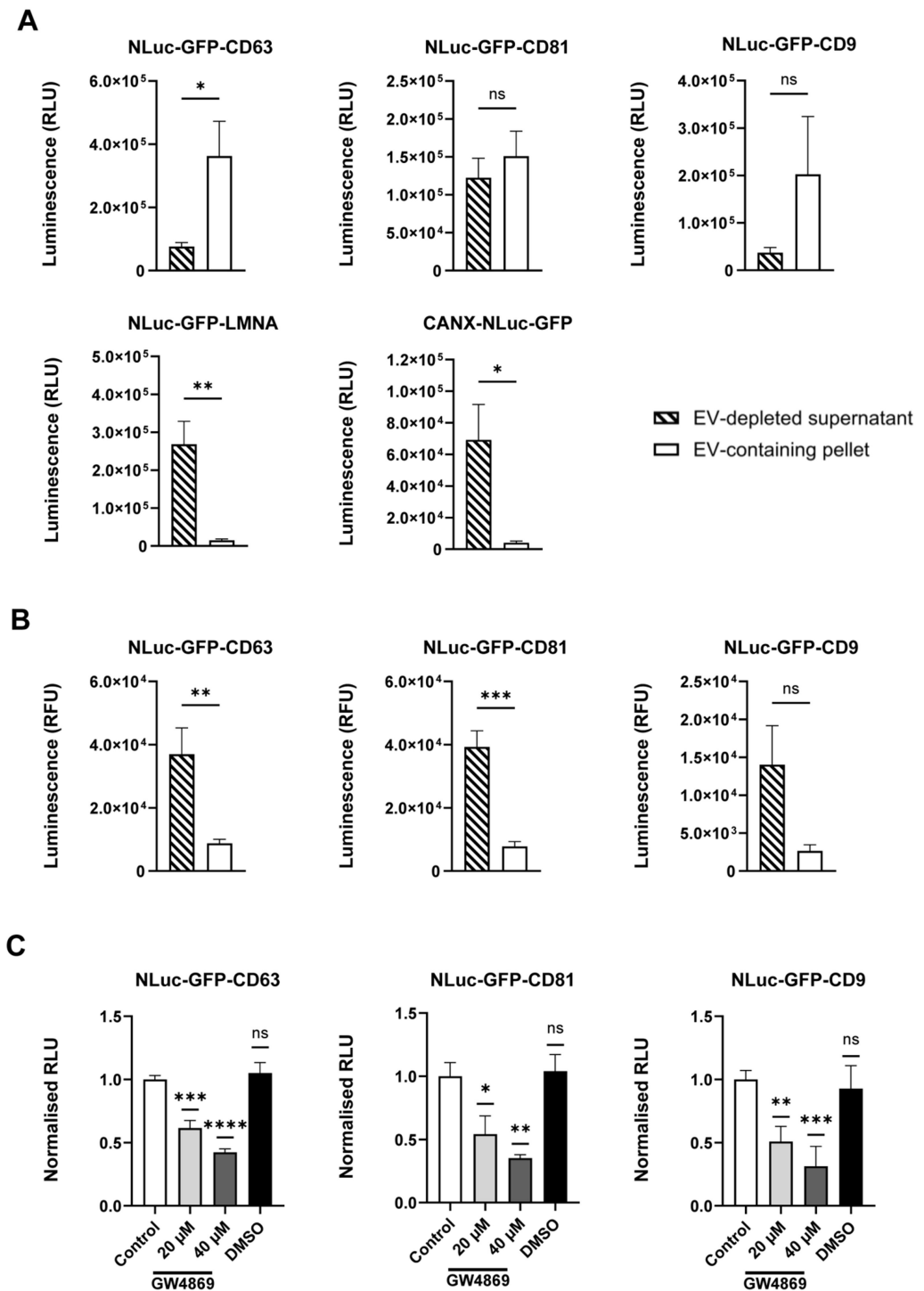
692 induced EVs; idEVs). Scale bar: 200 nm. **B)** Concentration of particles isolated from cell culture supernatants of
693 untreated or infected A549 cells at different time points. **C)** Size distribution of the isolated particles.
694 Concentration and sizes of isolated EVs were measured using NTA. **D)** Upset R plot showing the intersection of
695 proteins detected by LC-MS/MS proteomic analysis of EVs isolated from A549 cells either left untreated (EVs) or
696 infected with *A. fumigatus* (idEVs). Data obtained from 3 biological replicates. *, $p = <0.05$; **, $p = <0.01$; ns, not
697 significant.

698

**Fig 2.**

701 A) Scheme of the fusion proteins. The tetraspanins CD63, CD81, and CD9, and LMNA were N-terminally tagged
 702 while CANX was C-terminally tagged with a Nanoluciferase (NLuc) and a GFPSpark (short: GFP). B) CLSM analysis
 703

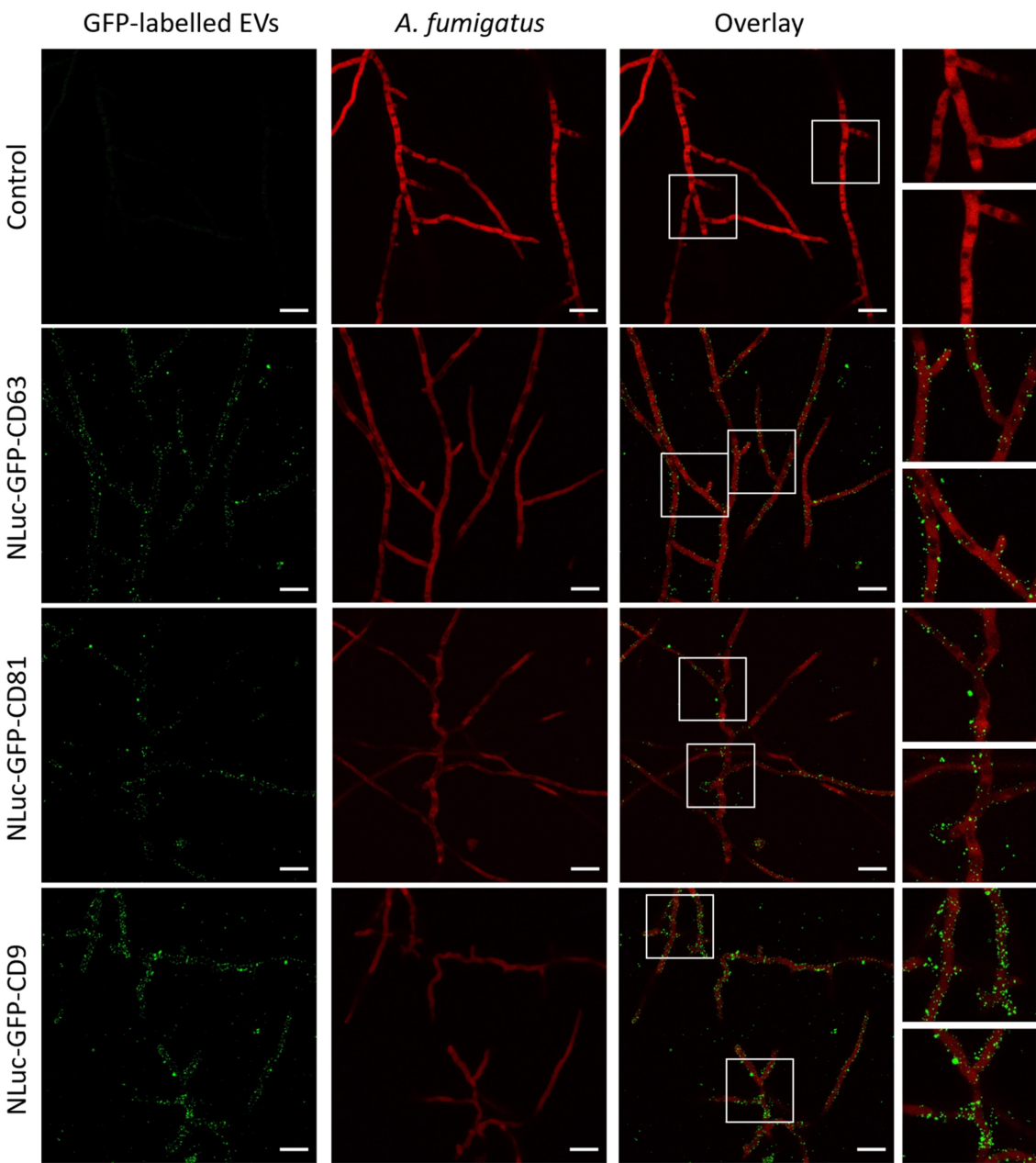
704 revealed the expression of the different tetraspanin fusion proteins within transfected A549 epithelial cells
705 based on the GFP signal. Non-transfected cells imaged with the same settings for GFP showed no background
706 signal or autofluorescence. Nuclei of the cells were stained with DAPI and the cell membrane was stained using
707 Cell Mask deep red. Scale bar: 10 µm. **C)** Measurement of the luminescence signal in the cell culture supernatant
708 of transfected cells. Positive signals were obtained for cells transfected with either of the plasmids encoding the
709 tetraspanin as well as control fusion proteins. Results were obtained from at least 4 biological replicates.
710



714 A) Measurement of the luminescence signal in the EV-depleted supernatant compared to the EV-enriched pellet
715 after EV isolation from transfected A549 epithelial cells using a polymer-precipitation based method. EV

716 isolation led to an increased luminescence signal deriving from the EV-containing pellet compared to the EV-
717 depleted supernatant in cases of cells expressing the tetraspanin fusion proteins. EV isolation from cell culture
718 media of cells expressing the LMNA and CANX control fusion proteins resulted in most of the signal deriving
719 from the EV-depleted supernatant. **B)** Measurement of the luminescence signal in the EV-depleted supernatant
720 and EV-containing pellet of A549 EVs treated with Triton X-100 prior to EV isolation. Lysis of EVs resulted in a
721 shift of the luminescence signal from the pellet to the supernatant. **C)** Measurement of the luminescence signal
722 in the EV-containing pellet after EV isolation from transfected A549 cells treated with GW4869 or DMSO as a
723 control. Treatment of cells with GW4869 resulted in a dose-dependent decrease of the luminescence signal in
724 the pellet. Results of isolated and lysed EVs were obtained from at least 4 biological replicates. Inhibitor assays
725 using GW4869 were performed as three biological replicates *, $p = <0.05$; **, $p = <0.01$; ***, $p = <0.001$, ****, p
726 = <0.0001 ; ns, not significant.

727

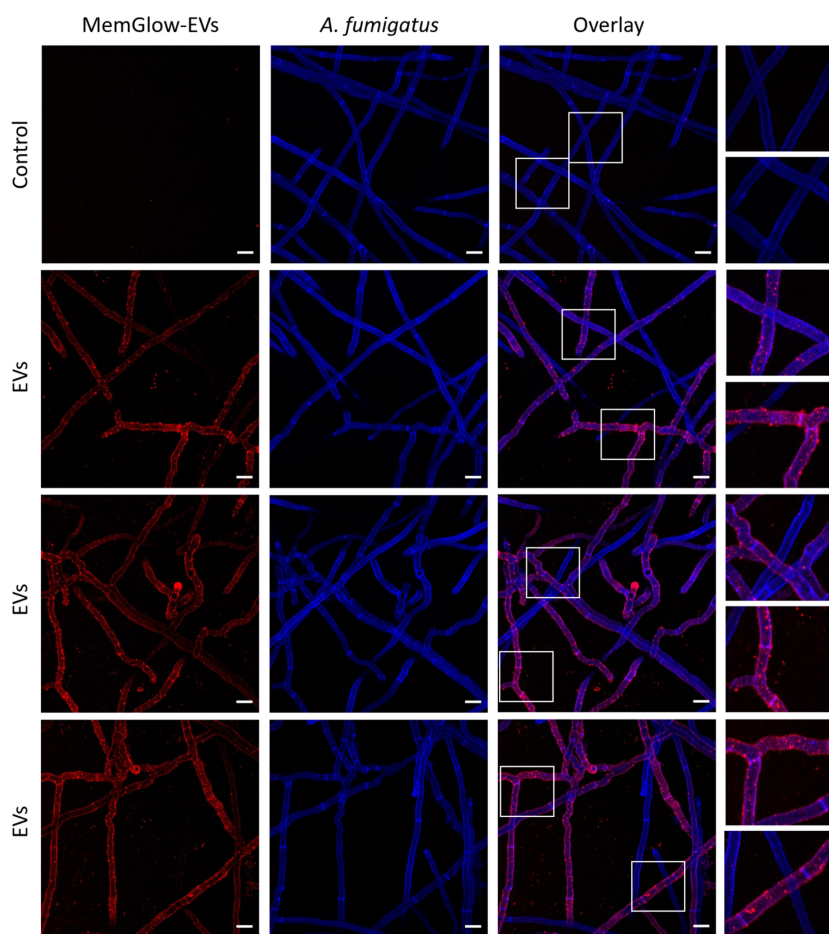


728

729 **Fig 4.**

730 CLSM images revealing that labelled A549 EVs can be visualised and are able to associate with *A. fumigatus*
731 hyphae. Resuspended EVs isolated from transfected cells expressing the NLuc-GFP-labelled tetraspanins were
732 added to 7 hour-old *A. fumigatus* dTomato germlings in a host cell-free system and incubated overnight. EVs
733 appeared as green-fluorescent dots with varying sizes. *A. fumigatus* treated with EVs isolated from non-
734 transfected cells were used a control. Images were taken using a Zeiss LSM 780 confocal microscope. Scale bar:
735 20 µm. Representative images from >3 biological replicates per construct.

736

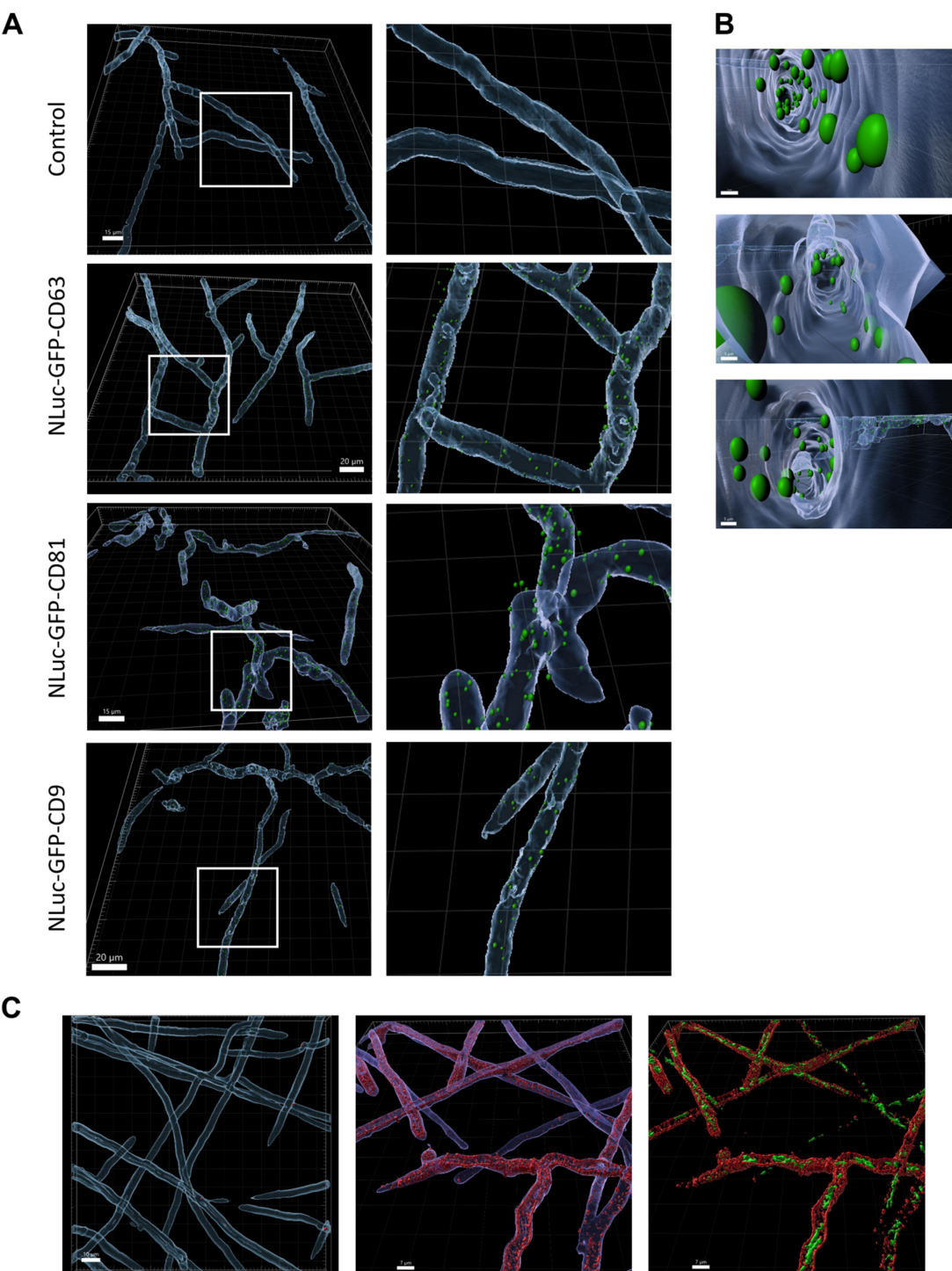


737

738 **Fig 5.**

739 Representative CLSM images of stained EVs co-localising with the *A. fumigatus* strain AfS35. EVs were isolated
 740 from non-transfected cells using size exclusion chromatography and stained with MemGlow 560 prior to
 741 addition to 7 hour-old *A. fumigatus* germlings in a host cell-free system. After overnight incubation hyphal cell
 742 walls were stained with calcofluor white (CFW) and subjected to CLSM. EVs appeared as red fluorescent dot-like
 743 signals with varying sizes. Control hyphae treated with MemGlow 560 in PBS exhibit no staining. Images were
 744 taken using a Zeiss LSM 780 confocal microscope. Scale bar: 20 μ m. Representative images from three biological
 745 replicates.

746

749 **Fig 6.**

750 **A)** 3D reconstruction of *A. fumigatus* hyphae CLSM images reveals the association of labelled EVs depicted as
 751 green dots with hyphae. Since the *A. fumigatus* AfS150/ pSK537 strain expressing a cytoplasmic dTomato
 752 protein was used here, the blue signal is equivalent with the limiting border of the hyphal lumen and thus the

753 hyphal membrane. **B)** Magnification of the 3D reconstructed hyphae confirms the association and partly
754 internalization of NLuc-GFP-tetraspanin labelled EVs into the hyphal lumen of *A. fumigatus*. **C)** MemGlow
755 stained EVs (in red) accumulate within *A. fumigatus* hyphae as a tube-like structure underneath the cell wall
756 (depicted in blue), likely accumulating at the hyphal cell membrane. The finding is supported upon the
757 reconstruction of the GFP-tagged mitochondria (in green).

758

759 REFERENCES

- 760 Abels, E. R., and X. O. Breakefield. 2016. 'Introduction to extracellular vesicles: biogenesis, RNA cargo selection,
761 content, release, and uptake', *Cell Mol Neurobiol*, 36: 301-312.
- 762 Amin, S., A. Thywissen, T. Heinekamp, H. P. Saluz, and A. A. Brakhage. 2014. 'Melanin dependent survival of
763 *Apergillus fumigatus* conidia in lung epithelial cells', *Int J Med Microbiol*, 304: 626-636.
- 764 Anderson, Corey L., Emma R. Langer, Timothy C. Routes, Seamus F. McWilliams, Igor Bereslavskyy, Timothy J.
765 Kamp, and Lee L. Eckhardt. 2021. 'Most myopathic lamin variants aggregate: a functional genomics
766 approach for assessing variants of uncertain significance', *npj Genomic Medicine*, 6: 103.
- 767 Bonsergent, Emeline, Eleonora Grisard, Julian Buchrieser, Olivier Schwartz, Clotilde Théry, and Grégory Lavieu.
768 2021. 'Quantitative characterization of extracellular vesicle uptake and content delivery within
769 mammalian cells', *Nat Commun*, 12: 1864.
- 770 Brakhage, A. A. 2005. 'Systemic fungal infections caused by *Aspergillus* species: epidemiology, infection process
771 and virulence determinants', *Curr Drug Targets*, 6: 875-886.
- 772 Brakhage, A. A., A. K. Zimmermann, F. Rivieccio, C. Visser, and M. G. Blango. 2021. 'Host-derived extracellular
773 vesicles for antimicrobial defense', *Microlife*, 2: uqab003.
- 774 Cai, Qiang, Lulu Qiao, Ming Wang, Baoye He, Feng-Mao Lin, Jared Palmquist, Sienna-Da Huang, and Hailing Jin.
775 2018. 'Plants send small RNAs in extracellular vesicles to fungal pathogen to silence virulence genes',
776 360: 1126-1129.
- 777 Cashikar, A. G., and P. I. Hanson. 2019. 'A cell-based assay for CD63-containing extracellular vesicles', *PLoS One*,
778 14: e0220007.
- 779 Catalano, M., and L. O'Driscoll. 2020. 'Inhibiting extracellular vesicles formation and release: a review of EV
780 inhibitors', *J Extracell Vesicles*, 9: 1703244.
- 781 Chuo, Steven Ting-Yu, Jasper Che-Yung Chien, and Charles Pin-Kuang Lai. 2018. 'Imaging extracellular vesicles:
782 current and emerging methods', *Journal of Biomedical Science*, 25: 91.
- 783 Corso, G., W. Heusermann, D. Trojer, A. Görgens, E. Steib, J. Voshol, A. Graff, C. Genoud, Y. Lee, J. Hean, J. Z.
784 Nordin, O. P. B. Wiklander, S. El Andaloussi, and N. Meisner-Kober. 2019. 'Systematic characterization of
785 extracellular vesicle sorting domains and quantification at the single molecule - single vesicle level by
786 fluorescence correlation spectroscopy and single particle imaging', *J Extracell Vesicles*, 8: 1663043.
- 787 Denning, D. W. 2024. 'Global incidence and mortality of severe fungal disease', *Lancet Infect Dis*.
- 788 Eppler, Felix, Verena Semmling, Cora Schild, Yahya Homsi, Shoshana Levy, Thorsten Lang, Christian Kurts, and
789 Waldemar Kolanus. 2011. 'CD81 is essential for the formation of membrane protrusions and regulates
790 Rac1-activation in adhesion-dependent immune cell migration', *Blood*, 118: 1818-1827.
- 791 Escobar, N., S. R. Ordonez, H. A. Wösten, P. J. Haas, H. de Cock, and H. P. Haagsman. 2016. 'Hide, keep quiet, and
792 keep low: Properties that make *Aspergillus fumigatus* a successful lung pathogen', *Front Microbiol*, 7:
793 438.
- 794 Escobar, Natalia, Ivan D. Valdes, Esther M. Keizer, Soledad R. Ordonez, Robin A. Ohm, Han A. B. Wösten, and
795 Hans de Cock. 2018. 'Expression profile analysis reveals that *Aspergillus fumigatus* but not *Aspergillus*
796 *niger* makes type II epithelial lung cells less immunological alert', *BMC Genomics*, 19: 534.
- 797 Essandoh, K., L. Yang, X. Wang, W. Huang, D. Qin, J. Hao, Y. Wang, B. Zingarelli, T. Peng, and G. C. Fan. 2015.
798 'Blockade of exosome generation with GW4869 dampens the sepsis-induced inflammation and cardiac
799 dysfunction', *Biochim Biophys Acta*, 1852: 2362-2371.
- 800 Ewald, J., F. Rivieccio, L. Radosa, S. Schuster, A. A. Brakhage, and C. Kaleta. 2021. 'Dynamic optimization reveals
801 alveolar epithelial cells as key mediators of host defense in invasive aspergillosis', *PLoS Comput Biol*, 17:
802 e1009645.
- 803 Fan, Yé, Cédric Pionneau, Federico Cocozza, Pierre-Yves Boëlle, Solenne Chardonnet, Stéphanie Charrin, Clotilde
804 Théry, Pascale Zimmermann, and Eric Rubinstein. 2023. 'Differential proteomics argues against a general
805 role for CD9, CD81 or CD63 in the sorting of proteins into extracellular vesicles', 12: 12352.

- 806 Görgens, A., M. Bremer, R. Ferrer-Tur, F. Murke, T. Tertel, P. A. Horn, S. Thalmann, J. A. Welsh, C. Probst, C.
807 Guerin, C. M. Boulanger, J. C. Jones, H. Hanenberg, U. Erdbrügger, J. Lannigan, F. L. Ricklefs, S. El-
808 Andaloussi, and B. Giebel. 2019. 'Optimisation of imaging flow cytometry for the analysis of single
809 extracellular vesicles by using fluorescence-tagged vesicles as biological reference material', *J Extracell
810 Vesicles*, 8: 1587567.
- 811 Gupta, D., X. Liang, S. Pavlova, et al. 2020. 'Quantification of extracellular vesicles in vitro and in vivo using
812 sensitive bioluminescence imaging', *J Extracell Vesicles*, 9: 1800222.
- 813 Hall, M. P., J. Unch, B. F. Binkowski, M. P. Valley, B. L. Butler, M. G. Wood, P. Otto, K. Zimmerman, G. Vidugiris, T.
814 Machleidt, M. B. Robers, H. A. Benink, C. T. Eggers, M. R. Slater, P. L. Meisenheimer, D. H. Klaubert, F.
815 Fan, L. P. Encell, and K. V. Wood. 2012. 'Engineered luciferase reporter from a deep sea shrimp utilizing a
816 novel imidazopyrazinone substrate', *ACS Chem Biol*, 7: 1848-1857.
- 817 Han, C., H. Kang, J. Yi, M. Kang, H. Lee, Y. Kwon, J. Jung, J. Lee, and J. Park. 2021. 'Single-vesicle imaging and co-
818 localization analysis for tetraspanin profiling of individual extracellular vesicles', *J Extracell Vesicles*, 10:
819 e12047.
- 820 Headland, Sarah E., Hefin R. Jones, Adelina S. V. D'Sa, Mauro Perretti, and Lucy V. Norling. 2014. 'Cutting-edge
821 analysis of extracellular microparticles using ImageStreamX imaging flow cytometry', *Sci Rep*, 4: 5237.
- 822 Heinekamp, T., H. Schmidt, K. Lapp, V. Pährtz, I. Shopova, N. Köster-Eiserfunke, T. Krüger, O. Kniemeyer, and A. A.
823 Brakhage. 2015. 'Interference of *Aspergillus fumigatus* with the immune response', *Semin Immunopathol*, 37: 141-152.
- 824 Hikita, T., M. Miyata, R. Watanabe, and C. Oneyama. 2018. 'Sensitive and rapid quantification of exosomes by
825 fusing luciferase to exosome marker proteins', *Sci Rep*, 8: 14035.
- 826 Hikita, T., M. Miyata, R. Watanabe, and C. Oneyama. 2020. 'In vivo imaging of long-term accumulation of cancer-
827 derived exosomes using a BRET-based reporter', *Sci Rep*, 10: 16616.
- 828 Jia, L. J., M. Rafiq, L. Radosa, P. Hortschansky, C. Cunha, Z. Cseresnyés, T. Krüger, F. Schmidt, T. Heinekamp, M.
829 Straßburger, B. Löffler, T. Doenst, J. F. Lacerda, A. Campos, Jr., M. T. Figge, A. Carvalho, O. Kniemeyer,
830 and A. A. Brakhage. 2023. '*Aspergillus fumigatus* hijacks human p11 to redirect fungal-containing
831 phagosomes to non-degradative pathway', *Cell Host Microbe*, 31: 373-388.e310.
- 832 Jia, Xiaodong, Fangyan Chen, Weihua Pan, Rentao Yu, Shuguang Tian, Gaige Han, Haiqin Fang, Shuo Wang, Jingya
833 Zhao, Xianping Li, Dongyu Zheng, Sha Tao, Wanqing Liao, Xuelin Han, and Li Han. 2014. 'Gliotoxin
834 promotes *Aspergillus fumigatus* internalization into type II human pneumocyte A549 cells by inducing
835 host phospholipase D activation', *Microbes and Infection*, 16: 491-501.
- 836 Józefowski, Szczenan, Maciej Czerkies, Anna Łukasik, Alicja Bielawska, Jacek Bielawski, Katarzyna Kwiatkowska,
837 and Andrzej Sobota. 2010. 'Ceramide and ceramide 1-phosphate are negative regulators of TNF- α
838 production induced by lipopolysaccharide', *The Journal of Immunology*, 185: 6960-6973.
- 839 Jun, Mi-Hee, Young-Wu Jun, Kun-Hyung Kim, Jin- A. Lee, and Deok-Jin Jang. 2014. 'Characterization of the
840 cellular localization of C4orf34 as a novel endoplasmic reticulum resident protein', *BMB reports*, 47.
- 841 Jurgielewicz, B. J., Y. Yao, and S. L. Stice. 2020. 'Kinetics and Specificity of HEK293T Extracellular Vesicle Uptake
842 using Imaging Flow Cytometry', *Nanoscale Res Lett*, 15: 170.
- 843 Kakarla, Ramesh, Jaehark Hur, Yeon Ji Kim, Jaeyoung Kim, and Yong-Joon Chwae. 2020. 'Apoptotic cell-derived
844 exosomes: messages from dying cells', *Experimental & Molecular Medicine*, 52: 1-6.
- 845 Köhler, J. R., B. Hube, R. Puccia, A. Casadevall, and J. R. Perfect. 2017. 'Fungi that infect humans', *Microbiol
846 Spectr*, 5.
- 847 Kowal, J., G. Arras, M. Colombo, M. Jouve, J. P. Morath, B. Primdal-Bengtson, F. Dingli, D. Loew, M. Tkach, and C.
848 Théry. 2016. 'Proteomic comparison defines novel markers to characterize heterogeneous populations
849 of extracellular vesicle subtypes', *Proc Natl Acad Sci U S A*, 113: E968-977.
- 850 Kulshreshtha, A., T. Ahmad, A. Agrawal, and B. Ghosh. 2013. 'Proinflammatory role of epithelial cell-derived
851 exosomes in allergic airway inflammation', *J Allergy Clin Immunol*, 131: 1194-1203, 1203.e1191-1114.
- 852 Latgé, J. P., and G. Chamilos. 2019. '*Aspergillus fumigatus* and aspergillosis in 2019', *Clin Microbiol Rev*, 33.

- 854 Lázaro-Ibáñez, E., F. N. Faruqui, A. F. Saleh, A. M. Silva, J. Tzu-Wen Wang, J. Rak, K. T. Al-Jamal, and N. Dekker.
855 2021. 'Selection of fluorescent, bioluminescent, and radioactive tracers to accurately reflect extracellular
856 vesicle biodistribution *in vivo*', *ACS Nano*.
- 857 Levy, Daniel, Mai Anh Do, Annie Brown, Kyle Asano, David Diebold, Hanzhe Chen, Jiayi Zhang, Brendan Lawler,
858 and Biao Lu. 2020. 'Chapter One - Genetic labeling of extracellular vesicles for studying biogenesis and
859 uptake in living mammalian cells.' in Sheila Spada and Lorenzo Galluzzi (eds.), *Methods in Enzymology*
860 (Academic Press).
- 861 Lionakis, M. S., R. A. Drummond, and T. M. Hohl. 2023. 'Immune responses to human fungal pathogens
862 and therapeutic prospects', *Nat Rev Immunol*, 23: 433-452.
- 863 Lischnig, A., M. Bergqvist, T. Ochiya, and C. Lässer. 2022. 'Quantitative proteomics identifies proteins enriched in
864 large and small extracellular vesicles', *Mol Cell Proteomics*, 21: 100273.
- 865 Loconte, L., D. Arguedas, R. El, A. Zhou, A. Chipont, L. Guyonnet, C. Guerin, E. Piovesana, J. L. Vázquez-Ibar, A.
866 Joliot, C. Théry, and L. Martín-Jaular. 2023. 'Detection of the interactions of tumour derived extracellular
867 vesicles with immune cells is dependent on EV-labelling methods', *J Extracell Vesicles*, 12: e12384.
- 868 Lőrincz Á, M., M. Schütte, C. I. Timár, D. S. Veres, Á Kittel, K. R. McLeish, M. L. Merchant, and E. Ligeti. 2015.
869 'Functionally and morphologically distinct populations of extracellular vesicles produced by human
870 neutrophilic granulocytes', *J Leukoc Biol*, 98: 583-589.
- 871 Loher, Jasmin, Tanja Breitschopf, Sven Krappmann, C. Oliver Morton, Maria Bouzani, Oliver Kurzai, Matthias
872 Gunzer, Mike Hasenberg, Hermann Einsele, and Juergen Loeffler. 2014. 'Human dendritic cell subsets
873 display distinct interactions with the pathogenic mould *Aspergillus fumigatus*', *International Journal of
874 Medical Microbiology*, 304: 1160-1168.
- 875 Lötvall, J., A. F. Hill, F. Hochberg, E. I. Buzás, D. Di Vizio, C. Gardiner, Y. S. Gho, I. V. Kurochkin, S. Mathivanan, P.
876 Quesenberry, S. Sahoo, H. Tahara, M. H. Wauben, K. W. Witwer, and C. Théry. 2014. 'Minimal
877 experimental requirements for definition of extracellular vesicles and their functions: a position
878 statement from the International Society for Extracellular Vesicles', *J Extracell Vesicles*, 3: 26913.
- 879 Mathieu, Mathilde, Nathalie Névo, Mabel Jouve, José Ignacio Valenzuela, Mathieu Maurin, Frederik J. Verweij,
880 Roberta Palmulli, Danielle Lankar, Florent Dingli, Damarys Loew, Eric Rubinstein, Gaëlle Boncompain,
881 Franck Perez, and Clotilde Théry. 2021. 'Specificities of exosome versus small ectosome secretion
882 revealed by live intracellular tracking of CD63 and CD9', *Nat Commun*, 12: 4389.
- 883 Mondal, A., K. A. Ashiq, P. Phulpagar, D. K. Singh, and A. Shiras. 2019. 'Effective visualization and easy tracking of
884 extracellular vesicles in glioma cells', *Biol Proced Online*, 21: 4.
- 885 Morandi, Mattia I., Petro Busko, Efrat Ozer-Partuk, Suman Khan, Giulia Zarfati, Yael Elbaz-Alon, Paula
886 Abou Karam, Tina Napso Shogan, Lana Ginini, Ziv Gil, Neta Regev-Rudzki, and Ori Avinoam. 2022.
887 'Extracellular vesicle fusion visualized by cryo-electron microscopy', *PNAS Nexus*, 1: pgac156.
- 888 Mulcahy, L. A., R. C. Pink, and D. R. Carter. 2014. 'Routes and mechanisms of extracellular vesicle uptake', *J
889 Extracell Vesicles*, 3.
- 890 Myhill, Nathan, Emily M. Lynes, Jalal A. Nanji, Anastassia D. Blagoveshchenskaya, Hao Fei, Katia Carmine
891 Simmen, Timothy J. Cooper, Gary Thomas, and Thomas Simmen. 2008. 'The subcellular distribution of
892 calnexin is mediated by PACS-2', *Molecular Biology of the Cell*, 19: 2777-2788.
- 893 Paris, S., E. Boisvieux-Ulrich, B. Crestani, O. Houcine, D. Taramelli, L. Lombardi, and J. P. Latgé. 1997.
894 'Internalization of *Aspergillus fumigatus* conidia by epithelial and endothelial cells', *Infect Immun*, 65:
895 1510-1514.
- 896 Paskevicius, Tautvydas, Rabih Abou Farraj, Marek Michalak, and Luis B. Agellon. 2023. 'Calnexin, more than just
897 a molecular chaperone', 12: 403.
- 898 Perez-Riverol, Yasset, Jingwen Bai, Chakradhar Bandla, David García-Seisdedos, Suresh Hewapathirana,
899 Selvakumar Kamatchinathan, Deepti J Kundu, Ananth Prakash, Anika Frericks-Zipper, Martin Eisenacher,
900 Mathias Walzer, Shengbo Wang, Alvis Brazma, and Juan Antonio Vizcaíno. 2022. 'The PRIDE database

- 901 resources in 2022: a hub for mass spectrometry-based proteomics evidences', *Nucleic Acids Research*,
902 50: D543-D552.
- 903 Rafiq, M., F. Rivieccio, A. K. Zimmermann, C. Visser, A. Bruch, T. Krüger, K. González Rojas, O. Kniemeyer, M. G.
904 Blango, and A. A. Brakhage. 2022. 'PLB-985 neutrophil-like cells as a model to study *Aspergillus*
905 *fumigatus* pathogenesis', *mSphere*, 7: e0094021.
- 906 Ricklefs, F. L., C. L. Maire, R. Reimer, *et al.* 2019. 'Imaging flow cytometry facilitates multiparametric
907 characterization of extracellular vesicles in malignant brain tumours', *J Extracell Vesicles*, 8: 1588555.
- 908 Ruf, D., V. Brantl, and J. Wagener. 2018. 'Mitochondrial fragmentation in *Aspergillus fumigatus* as early marker
909 of granulocyte killing activity', *Front Cell Infect Microbiol*, 8: 128.
- 910 Shopova, I. A., I. Belyaev, P. Dasari, *et al.* 2020. 'Human neutrophils produce antifungal extracellular vesicles
911 against *Aspergillus fumigatus*', *mBio*, 11.
- 912 Shpigelman, Jonathan, Fitzgerald S. Lao, Shiyin Yao, Chenyang Li, Tetsuya Saito, Fumi Sato-Kaneko, John P.
913 Nolan, Nikunj M. Shukla, Minya Pu, Karen Messer, Howard B. Cottam, Dennis A. Carson, Maripat Corr,
914 and Tomoko Hayashi. 2021. 'Generation and application of a reporter cell line for the quantitative
915 screen of extracellular vesicle release', 12.
- 916 Slivinschi, Bianca, Federico Manai, Carolina Martinelli, Francesca Carrieri, Camilla D'Amato, Martina Massarotti,
917 Giorgia Bresciani, Claudio Casali, Gloria Milanesi, Laura Artal, Lisa Zanoletti, Federica Milèlla, Davide
918 Arfini, Alberto Azzalin, Sara Demartis, Elisabetta Gavini, and Sergio Comincini. 2022. 'Enhanced delivery
919 of rose bengal by amino acids starvation and exosomes inhibition in human astrocytoma cells to
920 potentiate anticancer photodynamic therapy effects', *Cells*, 11: 2502.
- 921 Strohmeier, K., M. Hofmann, F. Hauser, D. Sivun, S. Puthukodan, A. Karner, G. Sandner, P. E. Le Renard, J. Jacak,
922 and M. Mairhofer. 2021. 'CRISPR/Cas9 genome editing vs. over-expression for fluorescent extracellular
923 vesicle-labeling: a quantitative analysis', *Int J Mol Sci*, 23.
- 924 Théry, C., K. W. Witwer, E. Aikawa, *et al.* 2018. 'Minimal information for studies of extracellular vesicles 2018
925 (MISEV2018): a position statement of the International Society for Extracellular Vesicles and update of
926 the MISEV2014 guidelines', *J Extracell Vesicles*, 7: 1535750.
- 927 Timár, C. I., A. M. Lorincz, R. Csépányi-Kömi, A. Vályi-Nagy, G. Nagy, E. I. Buzás, Z. Iványi, A. Kittel, D. W. Powell,
928 K. R. McLeish, and E. Ligeti. 2013. 'Antibacterial effect of microvesicles released from human
929 neutrophilic granulocytes', *Blood*, 121: 510-518.
- 930 Tognoli, M. L., J. Dancourt, E. Bonsergent, R. Palmulli, O. G. de Jong, G. Van Niel, E. Rubinstein, P. Vader, and G.
931 Lavieu. 2023. 'Lack of involvement of CD63 and CD9 tetraspanins in the extracellular vesicle content
932 delivery process', *Commun Biol*, 6: 532.
- 933 Trajkovic, K., C. Hsu, S. Chiantia, L. Rajendran, D. Wenzel, F. Wieland, P. Schwille, B. Brügger, and M. Simons.
934 2008. 'Ceramide triggers budding of exosome vesicles into multivesicular endosomes', *Science*, 319:
935 1244-1247.
- 936 van de Veerdonk, F. L., M. S. Gresnigt, L. Romani, M. G. Netea, and J. P. Latgé. 2017. '*Aspergillus fumigatus*
937 morphology and dynamic host interactions', *Nat Rev Microbiol*, 15: 661-674.
- 938 van Niel, G., G. D'Angelo, and G. Raposo. 2018. 'Shedding light on the cell biology of extracellular vesicles', *Nat
939 Rev Mol Cell Biol*, 19: 213-228.
- 940 Verweij, F. J., L. Balaj, C. M. Boulanger, *et al.* 2021. 'The power of imaging to understand extracellular vesicle
941 biology *in vivo*', *Nat Methods*, 18: 1013-1026.
- 942 Wang, S., B. He, H. Wu, Q. Cai, O. Ramírez-Sánchez, C. Abreu-Goodger, P. R. J. Birch, and H. Jin. 2024. 'Plant
943 mRNAs move into a fungal pathogen via extracellular vesicles to reduce infection', *Cell Host Microbe*, 32:
944 93-105.e106.
- 945 Welsh, Joshua A., Deborah C. I. Goberdhan, Lorraine O'Driscoll, *et al.* 2024. 'Minimal information for studies of
946 extracellular vesicles (MISEV2023): From basic to advanced approaches', *J Extracell Vesicles*, 13: e12404.
- 947 WHO. 2022. "WHO fungal priority pathogens list to guide research, development and public health action." In,
948 48.

- 949 Willms, E., H. J. Johansson, I. Mäger, Y. Lee, K. E. Blomberg, M. Sadik, A. Alaarg, C. I. Smith, J. Lehtiö, S. El
950 Andaloussi, M. J. Wood, and P. Vader. 2016. 'Cells release subpopulations of exosomes with distinct
951 molecular and biological properties', *Sci Rep*, 6: 22519.
- 952 Yáñez-Mó, M., P. R. Siljander, Z. Andreu, *et al.* 2015. 'Biological properties of extracellular vesicles and their
953 physiological functions', *J Extracell Vesicles*, 4: 27066.
- 954 Zhang, X., D. He, S. Gao, Y. Wei, and L. Wang. 2020. 'iTRAQ-based proteomic analysis of the interaction of A549
955 human lung epithelial cells with *Aspergillus fumigatus* conidia', *Mol Med Rep*, 22: 4601-4610.
- 956 Zhang, Zhihong, Rongyu Liu, Jacobien A. Noordhoek, and Henk F. Kauffman. 2005. 'Interaction of airway
957 epithelial cells (A549) with spores and mycelium of *Aspergillus fumigatus*', *Journal of Infection*, 51: 375-
958 382.
- 959